LANGMUIR

pubs.acs.org/Langmuir Article

Enhancement of Fluorescence Mediated by Silver Nanoparticles: Implications for Cell Imaging

Pradip Maiti, Swarupa Sarkar, Tanmoy Singha, Sannak Dutta Roy, Mrityunjoy Mahato, Parimal Karmakar, Sharmistha Paul, and Pabitra Kumar Paul*

Cite This: *Langmuir* 2023, 39, 6713–6729 Read Online

ACCESS | Metrics & More | Article Recommendations | Supporting Information

ABSTRACT: In this study, we report the surface enhanced fluorescence (SEF) of a biologically important organic dye, fluorescein (FL), by silver nanoparticles (Ag NPs) in an aqueous medium and its implications for human cell imaging. The as-synthesized Ag NPs were characterized by dynamic light scattering (DLS), zeta potential, transmission electron microscopy (TEM), and UV−vis absorption spectroscopic studies. The interaction and aggregation of FL dye with Ag NPs and a cationic surfactant, namely, cetyltrimethylammonium bromide (CTAB), were explored by UV−vis absorption and steady-state and time-resolved fluorescence spectroscopic methods. The distance-dependent fluorescence enhancement of FL due to Ag NPs in the solution was also theoretically correlated by three-dimensional finite-difference time-domain (3D-FDTD) simulation. The plasmonic coupling between neighboring NPs facilitated the augmentation of the local electric field, thereby producing various "hotspots" that influence the overall fluorescence of the emitter. J-type aggregates of FL in the presence of the CTAB micelles and Ag NP mixed solution were confirmed by electronic spectroscopy. The density functional theoretical (DFT) study revealed the electronic energy levels associated with different forms of FL dye in the aqueous solution. Most interestingly, the Ag NP/FL mixed system used in fluorescence imaging of human lung fibroblast cells (WI 38 cell line) showed a significantly stronger green fluorescence signal compared to that of FL after an incubation period of only 3 h. This study confirms that the Ag NP mediated SEF phenomenon of the FL dye is also manifested in the intracellular medium of human cells giving a brighter and more intense fluorescence image. The cell viability test after exposure to the Ag NP/FL mixed system was confirmed by the MTT assay method. The proposed study may have an implication as an alternate approach for human cell imaging with higher resolution and more contrast.

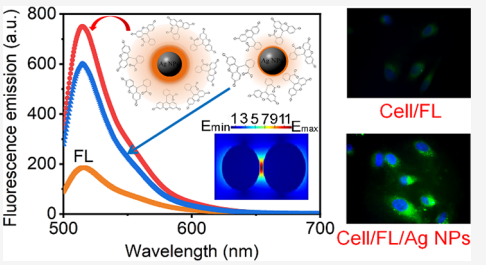

INTRODUCTION

A wide range of biomedical applications have been developed and commercially available with the advancement of fluorescence emission spectroscopic techniques, synthesis of a variety of new fluorescent compounds, as well as modern device sophistication. The synthesis of new organic and inorganic probe materials with unique physical and physicochemical properties has spurred the systematic investigation of protein localization and biological function of living cells.[1,2] Cellular imaging by the fluorescence technique is an excellent analytical approach that has revolutionized the molecular cell biology and related fields through the assessment or identification of the dynamical behavior of intra- or extracellular components of a variety of living cells in real time, i.e., by fluorescence imaging microscopy.

Fluorescence imaging microscopy is used in many biological assays because of its potentially high sensitivity, selectivity, and ease of use to understand the underlying causes of various diseases at the cellular and molecular level with very low invasiveness and insensitivity toward magnetic and electric signals.[3,4] Although fluorescence imaging microscopy has a long scientific history, this technique itself faces difficulties in case of fluorophores with low intrinsic light emission, low photostability, and photobleaching[5] as this method essentially demands fluorophores such as organic dyes, quantum dots, etc., with distinct spectral and photophysical properties. Many traditional organic fluorescent dyes are being used as probes in conventional fluorescence microscopy, but, their performance is still limited because of the low spatial and temporal resolution as well as the interference by the background autofluorescence from the cellular environments.[6,7] With the recent advancement of scientific research in the microscopic level, it is therefore very important to improve the performance and sensitivity of such fluorescence-based imaging method by enhancing the intrinsic fluorescence emission of the probes. In view of the performance of various fluorescence-based detection methods, plasmonic metal nanostructures such as

Received: January 21, 2023
Revised: April 19, 2023
Published: May 3, 2023

https://doi.org/10.1021/acs.langmuir.3c00204
Langmuir 2023, 39, 6713−6729

gold (Au), silver (Ag), platinum (Pt), copper (Cu), aluminum (Al), etc., are presently in active consideration for research among the scientific communities because of their novel optical functionalities and biocompatibility suitable for diverse applications, namely, biomolecular sensing, bioimaging, disease diagnosis, targeted drug or gene delivery, nanomedicine, etc.[8−11] Also, these metal nanostructures can efficiently modify both the excitation and emission properties of organic fluorophores in the vicinity of metal via coupling of the oscillating dipole of fluorophore and the plasmonic electric field of metal during photoexcitation. In general, this strategy aims for the augmentation of the local electromagnetic (EM) field intensity due to the photoexcitation of surface plasmons of the metal, thereby producing various "hotspots" in the nanogap region between neighboring nanoparticles (NPs) toward a variety of applications in nanophotonics.[12,13] Depending upon the suitable combination of fluorophore and metal and their relative distance in the metal−fluorophore ensemble, the radiative decay rate and photostability may be increased, resulting in a concomitant increase in the overall steady-state fluorescence emission, which is referred to as the metal enhanced fluorescence (MEF). Recently, MEF, also known as surface enhanced fluorescence (SEF) or plasmon enhanced fluorescence (PEF), of various organic fluorophores has attracted great attention from researchers in the field of fluorescence microscopy to circumvent the downsides by enhancing the fluorescence emission with a high signal-to-noise ratio.[4,14]

Drexhage[15] in 1974 first reported the origin of metal-based SEF when fluorophores placed within close proximity to metal NPs induce localized surface plasmon resonance (LSPR). LSPR is originated around the surface of metal NPs when an incident light excites the free surface electrons of metal NPs, producing a strong near-field due to coherent oscillation of the photoexcited surface electrons.[16] This evanescent field of surface plasmons decays exponentially with the distance of the order of 10−200 nm from the metal NP surface.[16] This strong SEF is obtained when the localized surface plasmons of metal NPs are strongly coupled with the molecular electronic transition dipole of fluorophores resulting in the overall enhancement of fluorescence.[16] However, such near-field enhancement should depend upon the inter-NP separation as well as different nanoarchitectures of plasmonic metals.[8,9] Bhaskar et al.[17] reported nanovoids and nanocrevices created by silver Soret colloid (Ag-SCs) in a surface plasmon-coupled emission (SPCE) platform for highly directional local field enhancement that facilitates 104-fold enhanced fluorescence signal of organic emitters and has been successfully utilized for femtomolar-level sensing of glutathione. Nanoengineered heteroatomic hybrid nanoassemblies such as AgAu, $AuSiO_2$, etc., with robust LSPR in an SPCE platform have also been reported for enhanced and highly polarized fluorescence emission.[18,19] Another exciting approach has recently been developed where exceptional augmentation of optical energy occurred in the hot spots created between plasmonic Ag NPs and one-dimensional photonic crystal (1DPhC) in a photonic crystal-coupled emission (PCCE) platform resulting in a 200-fold fluorescence enhancement of an organic emitter, which has been judiciously adopted for sensing of environmental Al^{3+} ion at a femtomolar limit of detection in drinking water samples.[20] On the other hand, when the fluorophore is directly adsorbed on the NP surface or located at very short distances from the metal surface, quenching of fluorescence emission takes place because of nonradiative energy transfer to the surface plasmon of metal NPs.[21] Again, no fluorescence enhancement is observed when the fluorophores are far from the NP surface. Therefore, the optimization of the distance between metal NP surface and the fluorophores is very crucial to obtain effective SEF.[22] Among the various metal NPs, Ag NPs and their various types of core−shell structures[23] have been widely used as a source of LSPR for SEF because of their interesting properties such as ease of surface modification for high electron conductivity linked with their advanced reactivity, high reflection, and suitability arising from the nanoparticles' higher surface area to volume ratio when compared to their bulk solid form.[24] The SEF phenomenon of organic dyes is very sensitive to Ag NP concentrations in aqueous media. Additionally, because of the high surface zeta (ζ) potential, Ag NPs are mostly stable in their aqueous colloidal dispersion.[8] As Ag NPs do not show any intrinsic fluorescence, the SEF of organic dyes due to their interaction with Ag NPs greatly motivates the present research for the application in human cell imaging. However, a detailed understanding of the interactions of nanoparticles' LSPR with organic fluorophore and the related photophysical behavior is extremely important for the realization of applications of SEF in the field of bioimaging.

Organic fluorophores such as xanthene dyes have been widely used as fluorescent probes, laser dyes, nonlinear optics, biological probes, etc.[25] Among the various xanthene dyes, water-soluble fluorescein (abbreviated as FL) is a very essential nontoxic dye that shows high sensitivity to the micro milieu, good solubility in water, and distinct spectral properties.[26−28] Depending on the pH of the solution, FL may exist in different tautomeric forms, which make it a model molecule for different adsorption experiments.[29] Because of the high sensitivity toward biopolymers, FL dye is vastly used as a fluorescent agent in the field of disease diagnosis, staining of biological specimens, cell screening in bioimaging, and specific drug delivery.[30,31] Although FL is a well-studied organic fluorophore, the information regarding the SEF of this dye due to Ag NPs in aqueous media for possible applications in human cell imaging is limited. It is also relevant to mention that real human cells contain a variety of surfactants such as surfactant proteins (SP-A, SP-B, SP-C, etc.).[32] So, for cellular imaging studies with FL dye, it is of prior importance to study the interaction of FL dye molecules with a model surfactant to anticipate their association or aggregation behavior while interacting with surfactants because the aggregation or association of dye molecules eventually may disrupt their translocation through the cell membrane and also the intrinsic fluorescence signal of the emitter molecules during cellular imaging. Therefore, a detailed study of the photophysical characteristics and aggregation behavior of FL molecules in the presence of metal NPs and a surfactant is of utmost importance for both fundamental and technological interests.

This present study focuses on the SEF phenomenon of FL dye molecules due to Ag NPs in aqueous solutions and its implication for imaging of human lung fibroblast cells (WI 38 cell line) as well as the aggregation behavior of FL in pre- and postmicellar solution of a cationic surfactant, namely, cetyltrimethylammonium bromide (CTAB). Ag NPs are synthesized by the chemical reduction method and are characterized by UV−vis absorption, dynamic light scattering (DLS), ζ potential, and transmission electron microscopy (TEM) techniques. UV−vis absorption and steady-state and

https://doi.org/10.1021/acs.langmuir.3c00204
Langmuir 2023, 39, 6713−6729

time-resolved fluorescence emission spectra of the Ag NP/FL mixed solution give an indication of the formation of dianionic species of FL dye from the monoanionic form in the aqueous solution in the presence of Ag NPs. The aggregates of FL are formed because of strong electrostatic interactions between CTAB and FL in the aqueous solution. The nature of aggregates depends upon the molecular dipole orientations that are reflected in the UV−vis absorption spectrum. In this study, J-type aggregates of FL are observed in the presence of the colloidal Ag NP and CTAB micellar solution. Also, nanoparticles' concentration dependent SEF of FL dye is further correlated with the results obtained by three-dimensional finite-difference time-domain (3D-FDTD) theoretical simulations. The density functional theoretical (DFT) calculations reveal the electronic properties of various molecular species of FL dye, which are consistent with the observed spectroscopic results. The Ag NP/FL mixed solution has been incorporated in the culture medium of live human lung fibroblast cells for efficient cell imaging. Also, the cytotoxicity study using the 3-[4,5-dimethylthiazol-2-yl]-2,5 diphenyl tetrazolium bromide (MTT) assay method reveals no significant toxicity of the proposed Ag NP/dye based probe system for cell imaging.

EXPERIMENTAL SECTION

Materials used and the synthesis of Ag NPs are described in detail in the Supporting Information.

Cell Line and Culture Conditions. Human lung fibroblast cells (WI 38 cell line) were cultured in an enriched cell culture medium of MEM supplemented with 10% FBS, 1% mixture of antibiotics (penicillin and streptomycin), 1% antioxidant (L-glutamine), 1% MEM nonessential amino acids (NEAA), 1% MEM amino acids, and 1% MEM vitamin solution. The cells were maintained at a temperature of 310 K in the prevalence of 5% carbon dioxide (CO_2) and 95% relative humidity (RH). The cytotoxicity study of Ag NP, FL, and Ag NP/FL systems was performed by using the MTT assay method. At first, cells were cultured in well plates at a density of 2×10^5 cells per well, and different volumes of Ag NP, FL, and Ag NP/FL mixed solutions were added to each well. Concentrations of Ag NPs in the cell culture medium for the MTT assay were 0, 0.006, 0.008, and 0.01 nM, respectively, whereas the concentrations of FL dye were 0, 0.8, 1, and 2 μM, respectively. Ag NP/FL mixed solutions were prepared by mixing Ag NPs and FL solution in a 1:1 volume ratio. After 3 h of incubation, the MTT reagent solution (450 μg/mL) was added to each well and further incubated for 3 h. The MTT solution was then removed from the culture medium, and subsequently, the MTT solubilization buffer was added to each well. Finally, the formation of formazol crystal color was monitored by measuring the absorbance at 570 nm using a microplate reader (BioTek, USA).

Protocol of Human Cell Imaging. The human lung fibroblast cells (WI 38 cell line) at a density of 2×10^5 cells per cm^3 were cultured on coverslips (3.5 × 3.5 cm) for a period of 20 h at 310 K, 5% CO_2, and 95% RH. Then, these cells were exposed separately to 150 μL of FL and Ag NP/FL mixed solution (in a 1:1 volume ratio) and incubated for another 3 h in the same ambient conditions. To avoid any contaminations, the cells were fixed and thoroughly washed with the help of 4% paraformaldehyde and 1× PBS (phosphate buffer saline) buffer. Finally, the coverslips having cells were mounted with 1× DAPI (4′,6-diamidino-2-phenylindole) mounting media and sent for the microscopic analysis. Fluorescence microscopy studies were carried out with a Leica DMLB (Germany) fluorescence microscope under 100× magnification. Quantification analysis was performed using the ImageJ software.

COMPUTATIONAL DETAILS

The geometry optimizations and quantum-chemical calculations of different species of FL dye in the solvent medium (water) were carried out by the density functional theory (DFT) using the Gaussian 09 suit of software package.[33] Initially, the geometries of different structural forms were optimized in a vacuum using the B3LYP functional (Becke's three-parameter (B3) functional with Lee−Yang−Parr (LYP) hybrid correlation energy)[34] and 6-31 + G basis set.[34] The obtained geometries were then used as the beginning point for optimization in the water medium at the same level of theory. Water was modeled as an implicit solvent using the integral equation formalism polarizable continuum model (IEFPCM) at room temperature (298 K), and further calculations were performed using the B3LYP/6-31G and B3LYP/6-31 + G level of theory.[34] The geometry optimized structures of different forms of FL dye were obtained by the fully relaxed method, and their corresponding molecular orbitals such as HOMO and LUMO levels were visualized using the GaussView 6.0.16 software package.[35] After each geometry optimization, frequency checks were carried out to confirm that local minima on the potential energy surfaces were established. The transition dipole moments (μ) were determined using time dependent density functional theory (TD-DFT) with the same exchange correlation function and basis sets as were used for geometry optimization.

The 3D-FDTD theoretical simulation was performed using the FDTD software (Lumerical Solutions Software)[36] to calculate the spatial distribution of electric field intensities due to localized surface plasmons of Ag nanoaggregates under photoillumination of suitable wavelength. Within the 3D simulation space, a minimal mess size, i.e., 0.1 × 0.1 × 0.1 nm in *X*-, *Y*-, and *Z*-directions, respectively, was selected for mapping the surface boundaries of the NPs. From these parameters, the resolutions of the simulations were determined by creating the 3D cube messes using the in-built machine features of the software. The material properties of the Ag used and the solvent (water, RI ∼1.33) were incorporated from the software in-built database.[37] The particle size and the separation between two consecutive NPs as obtained from the TEM images were included in the simulation. The plane-polarized EM wave having wavelength in the range of 200 to 700 nm with an electric field of amplitude ∼1.0 V m^{-1} was used to excite Ag nanoaggregates, leading to the augmentation of the maximum local electric field. The estimation of the optical responses of the metal NPs was based on the Mie theory and Total Field Scattered Field (TFSF) source in the 3D-FDTD simulation approach. To maximize the resolution of the field enhancement regions around Ag NPs and also to minimize simulation time, perfectly matched layer (PML) boundary conditions were introduced to avoid reflection and back scattering of the electric field from the preselected boundary. A 3D monitor was placed in the simulation space to record the data and visualize the theoretically simulated result for each calculation. To confirm the full convergence of the incident electric field, the overall simulation time was fixed at 500 fs. After completion of simulation, we observed various electric field "hotspots" that were confined predominantly in the nanogap spaces between the NPs.

https://doi.org/10.1021/acs.langmuir.3c00204
Langmuir 2023, 39, 6713−6729

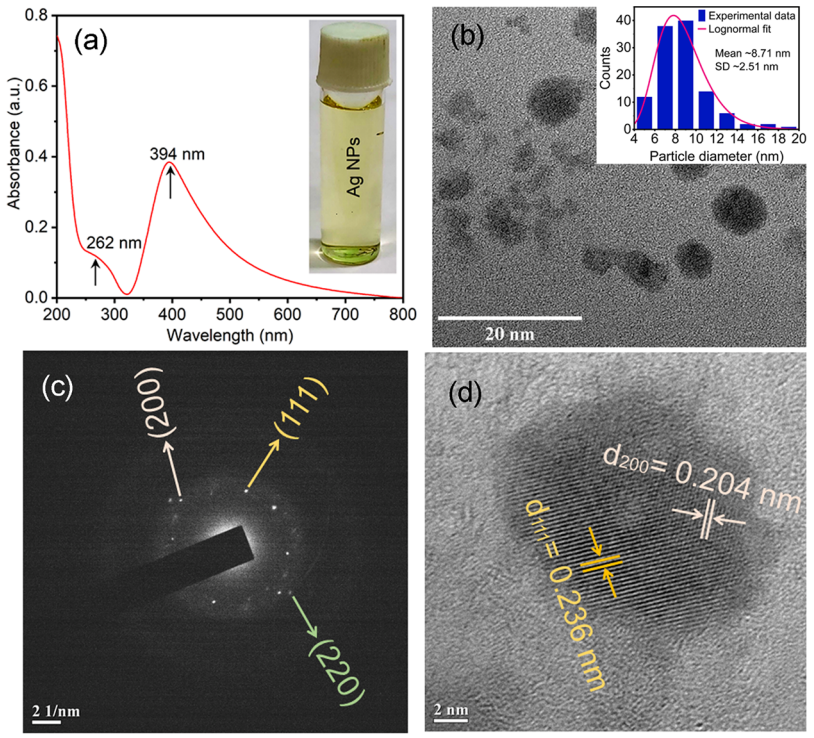

Figure 1. (a) UV−vis absorption spectrum of Ag NP aqueous dispersion. (b) TEM image, (c) SAED pattern with lattice plane indices, and (d) HRTEM with crystal spacing of as-synthesized Ag NPs. Insets of panels a and b show the glass vial containing bright yellow colored colloidal Ag NP dispersion and the lognormal particle size distribution, respectively.

RESULTS AND DISCUSSION

Characterization of Ag NPs. The optical, morphological, and surface potential characterizations of as-synthesized Ag NPs were explored by UV−vis absorption spectroscopy, HRTEM, DLS, and ζ potential measurements, respectively. The detailed characterizations methods are discussed in the Supporting Information. The UV−vis absorption spectrum of Ag NP aqueous colloidal dispersion is shown in Figure 1a. The absorption spectrum exhibits a strong band centered at around ∼394 nm along with an additional shallow shoulder at around ∼262 nm. The sharp and distinct band observed at ∼394 nm in the absorption spectrum is corroborated with the LSPR of Ag NPs in the aqueous medium.[32] The high-energy band observed at ∼262 nm is associated with the intraband electronic transition of silver, which is also reported for the other noble metal NPs.[38] These distinct absorption peaks of Ag NPs led us to investigate several interesting applications such as SEF of organic fluorescent guest molecules placed in nanoscale proximity of the metal surface.

The DLS spectrum as presented in Figure S1a (Supporting Information) of the Ag NP colloidal aqueous solution shows a bimodal size distribution with two distinct peaks that originated from the anisotropic geometries of NPs leading to two different rotational and translational diffusion constants in the light scattering measurements.[39] The higher value (∼0.74) of polydispersibility index (PDI) as obtained by the DLS study also reveals the different sized Ag NPs in the medium. The average hydrodynamic diameter of Ag NPs was found to be ∼10.78 nm. Also, to have a knowledge about the stability of Ag NP colloidal dispersion, the surface ζ potential was measured at an ambient condition (Figure S1b) and found to be −21.7 mV. This result indicates that the NPs could overcome the weak van der Waals attractions through strong electrostatic repulsions between the anionic borohydride coronas around the NP surface and remained effectively stabilized because of their very high value of negative ζ potential. To understand the nanoscale features such as origin of multiple absorption peaks of Ag NPs and their remarkable role toward the SEF of FL dye, the HRTEM study along with d-spacing identifications and SAED pattern was carried out. The TEM micrograph of as-synthesized Ag NPs as shown in Figure 1b reveals the nearly spherical, nonuniform size distribution of NPs, and their average diameter is estimated as ∼8.71 nm from the lognormal size distribution curve (inset of Figure 1b and Figure S2a) with a standard deviation (SD) of ∼2.51 nm. The heterogeneous size distribution of Ag NPs may be due to the different rates of nucleation of individual NPs in the ensemble. Because the change in surface area to volume ratio during the growth of Ag NPs should depend upon the time which may vary with the macroscopic conditions involved in the nucleation and growth process.[40] The SAED pattern and HRTEM image (Figure 1c,d) clearly indicate different d-spacings and lattice fringes that are oriented in different directions. The d-spacing values of the diffraction planes (Figure 1c) (from inside to out) are estimated as ∼0.23683 nm (d_{111}), ∼0.20494 nm (d_{200}), and ∼0.14802 nm (d_{220}), which are also identified and represented in the HRTEM image (Figure 1d). These crystallographic signatures of Ag NPs are in good agreement with the face centered cubic (FCC) structure according to the standard crystallography of silver (JCPDS card no. 04-0783).[41,42]

These mixed orientations of the fringes are known to be responsible for LSPR mediated localized EM near-field distributions that largely contribute in the SEF phenomenon and are further correlated by 3D-FDTD simulations study as discussed later.

https://doi.org/10.1021/acs.langmuir.3c00204
Langmuir 2023, 39, 6713−6729

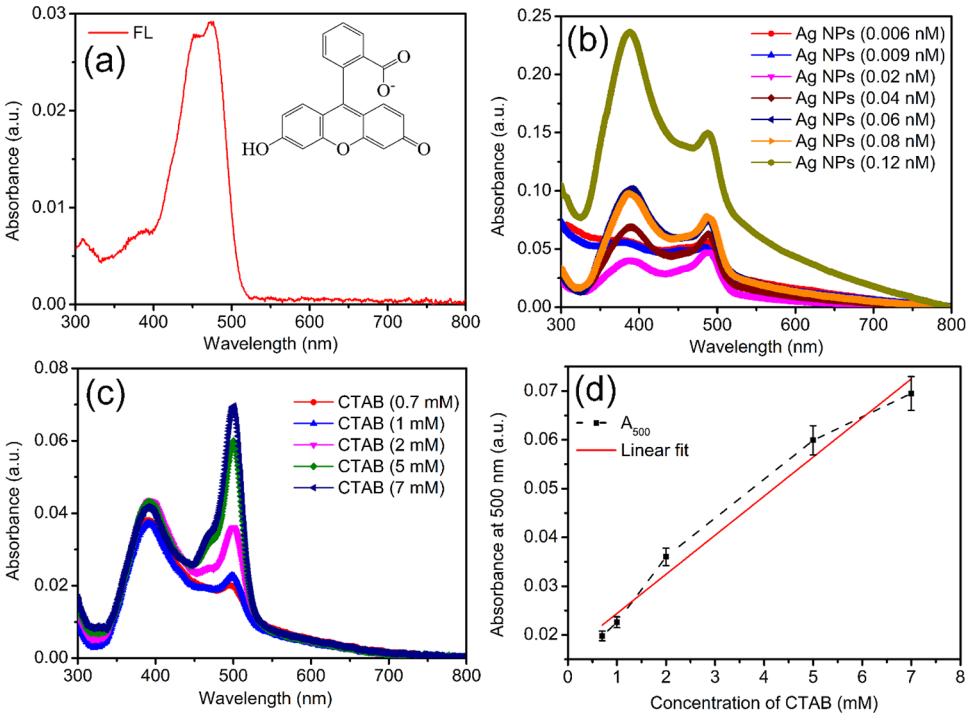

Figure 2. (a) UV−vis absorption spectrum of the aqueous solution of FL dye (concentration of 10 μM). UV−vis absorption spectra of (b) Ag NP/FL mixed solutions for different concentrations of Ag NPs and (c) Ag NP/FL mixed solution in the presence of CTAB. The concentrations of Ag NPs and FL dye were 0.04 nM and 10 μM. (d) Plot of absorbance intensity of the Ag NP/FL/CTAB mixed system vs concentration of the CTAB solution. Inset of panel a shows the molecular structure of FL monoanionic species.

The molar concentration of as-synthesized Ag NPs was calculated by a method described in the literature.[43] For this purpose, first, the number of silver atoms per nanoparticle (n_{Ag}) was calculated by using eq 1.[43]

$$n_{Ag} = \frac{\pi \rho N_A}{6M} d_{av}^3 \quad (1)$$

where ρ is the density of FCC silver (10.5 g cm^{-3}), N_A is Avogadro's number (6.023×10^{23}), M is the atomic mass of silver (107.868 g), and d_{av} is the mean diameter of the NPs. Thus, in this case, an Ag NP of average diameter ~8.71 nm is composed of ~20,204 silver atoms. The molar concentration (C) of the Ag NP colloidal dispersion was determined by using eq 2.[43]

$$C = \frac{N_T}{V n_{Ag} N_A} \quad (2)$$

where N_T is the total number of silver atoms added as $AgNO_3$ in the reaction mixture (whose value is $\sim 2.409 \times 10^{18}$ for 80 mL of 0.05 mM $AgNO_3$ solution), V is the total volume of the reaction solution in liters (0.206 L), and n_{Ag} is the concentration of silver atoms in each Ag NP (which is ~20,204 as obtained from eq 1). The calculated molar concentration of the Ag NP aqueous colloidal dispersion is ~0.96 nM at 298 K, and its molar extinction coefficient (ε) was determined by using the well-known Beer−Lambert law as described by eq 3.[44]

$$\varepsilon = \frac{A}{Cl} \quad (3)$$

where A is the absorbance at maximum absorption wavelength (394 nm) (Figure 1a); l is the sample path length, which is 1 cm in our measurements; and C is the molar concentration of the Ag NP colloidal dispersion as obtained by eq 2. The calculated value of ε is $\sim 4.003 \times 10^8$ M^{-1} cm^{-1} and is consistent with the data reported in the literature.[44] The high value of ε indicates that the synthesized Ag NPs are highly capable to respond to optical excitation.

UV−Vis Absorption Spectroscopic Studies. Figure 2a shows the UV−vis absorption spectrum of the aqueous solution of pure FL dye (concentration of 10 μM) at room temperature (298 K), and the pH of the solution was measured as ~5.8. The preparation of the solutions and characterization techniques are highlighted in the Supporting Information. It is observed that FL shows a strong absorption band with a peak centered at ~472 nm ($\varepsilon_{472\ nm}$ = 29,000 M^{-1} cm^{-1}) along with a closely spaced high-energy band with a peak centered at ~454 nm and a weak shoulder observed at around ~390 nm. Both the absorption bands (~472 and ~ 454 nm) are attributed to the existence of monoanionic species of FL in the aqueous solution and are consistent with the results reported elsewhere.[28] The observed weak shoulder at ~390 nm may be due to the presence of a small fraction of neutral species of FL in the aqueous solution.[28] The literature also reveals that in aqueous environments, FL can exist in different ionic forms such as cation, neutral, monoanion, and dianion depending upon the pH of the medium,[45] and their respective chemical structures are shown in Figure S3. The conversion mechanism of the FL dye molecule from a monoanion to a dianion is also shown in Figure S4. These different ionic structures correspond to various absorption and fluorescence emission properties of FL dye. In this study therefore, the change of pH of the solvent medium after addition of FL dye in the solution plays an important role in the observed absorption and fluorescence properties that are mostly attributed to its monoanionic form.

https://doi.org/10.1021/acs.langmuir.3c00204
Langmuir 2023, 39, 6713−6729

We also studied the effect of Ag NP colloidal dispersion on the absorption spectrum of FL in an aqueous solution. Figure 2b represents the UV−vis absorption spectra of the FL aqueous solution (concentration of 10 μM) in the presence of Ag NPs with varying concentrations, viz., 0.006, 0.009, 0.02, 0.04, 0.06, 0.08, and 0.12 nM. The pH of the mixed solution was measured as ∼8.7. It is observed from the figure that after addition of Ag NP colloidal dispersion to the FL dye solution, the monoanionic monomeric band is red-shifted to ∼490 nm, and with the increase in Ag NP concentrations in the mixed solutions, the absorbance intensity at ∼490 nm gradually increases. The absorption peak observed at ∼388 nm is attributed to the plasmonic oscillation of Ag NPs after photoexcitation, and the intensity of this band increases with the increase in the concentration of NPs. The slight change in the peak position of Ag NPs in the presence of FL dye may be due to some changes in the microenvironment around the NP surface in the aqueous medium. Most interestingly, the red-shift of the absorption band of FL when compared to the pure aqueous solution is probably due to the conversion of the monoanionic form of dye molecules to the dianionic form after the addition of Ag NPs.[46] This study also reveals that the effective pH of the mixed solution was increased because of Ag NPs when compared to that of the pure FL dye solution (pH ∼5.8) in the present experimental condition. Therefore, the change in the microenvironment due to the presence of Ag NPs causes the transformation of FL dye from monoanionic to dianionic species.[46] The increase in absorbance intensity of the Ag NP/FL mixed solution with the increase in Ag NP concentrations is probably due to the increase in plasmonic coupling between Ag NPs and FL dye molecules during the optical excitation. We also deconvoluted the absorption spectra of the Ag NP/FL mixed solution as shown in Figure S5, and it is found that the oscillator strength (f) and the transition dipole moment (μ) are increased for various concentrations of Ag NPs in the mixed solution. These parameters are summarized in Table S1.

Figure 2c shows the UV−vis absorption spectra of the mixed solution of Ag NPs (concentration of 0.04 nM) and FL (concentration of 10 μM) in the presence of aqueous solutions of the cationic surfactant CTAB with different concentrations, viz.,: 0.7, 1, 2, 5, and 7 mM. The chemical structure of CTAB is shown in Figure 3a. It is observed that a new absorption band

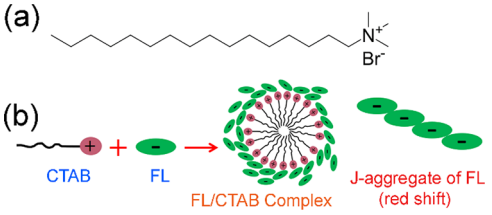

Figure 3. (a) Molecular structure of CTAB. (b) Schematic representation of the formation of J-type dye aggregates in the CTAB micellar medium.

of FL is developed at ∼500 nm in the absorption spectra of the Ag NP/FL/CTAB mixed solution. However, there is no appreciable change in the band position of the absorption maximum (∼472 nm) of FL observed except for some change in the intensity distribution. As CTAB forms a cation in the aqueous solution, the absorption band observed at ∼472 nm of FL might be due to the presence of some fraction of monoanionic monomeric species. Also, there is a small change in the absorbance intensity of the band at ∼390 nm (which arises due to the presence of Ag NPs in the mixed solution) with the increase in CTAB concentrations. This slight change in the absorbance may be attributed to the different surrounding microenvironment of Ag NPs in the mixed solution after addition of CTAB molecules. It is also evident from Figure 2d that the absorbance at ∼500 nm almost linearly increases with the increase in CTAB concentrations in the mixed solution. This implies that the anionic FL molecules can form a complex with cationic CTAB molecules via strong electrostatic interactions. As we have already assumed that in the presence of Ag NPs, most of the dye species were dianionic in the mixed solution, it may be presumed that the enhanced electrostatic interaction between FL and CTAB results in closer association of dye molecules that were attached with the polar part of CTAB molecules. As a consequence, the enhanced dipole−dipole interaction of dye molecules facilitates the formation of dye aggregates, which is reflected as the emergence of a new red-shifted absorption band at ∼500 nm compared to the monomeric dianionic band (∼490 nm). This red-shifted band is most possibly due to the formation of J-type dimer or aggregates of FL dianionic species in the studied aqueous medium.[47] We further examined the UV−vis absorption spectra of the FL solution (concentration of 10 μM) in the presence of CTAB of varying concentrations (viz., (in mM) 0.7, 1, 2, 5, 7, etc.) as shown in Figure S6a. We immediately observe that the absorbance of FL increases with the increase in CTAB concentrations. In fact, with the increase in CTAB concentrations, the number of available cationic binding sites increases, causing more dye molecules to form their aggregates due to their closer association. As a result, the absorption band intensity at ∼500 nm increases as a result of the increased number of dimeric species (J-type) in the mixed solution. The strength of the binding interaction of FL and CTAB in the Ag NP/FL/CTAB mixed solution can be described by the equilibrium constant or association constant (K_{eq}) using the modified Benesi−Hildebrand (BH) equation.[48]

$$\frac{1}{(A_x - A_0)} = \frac{1}{(A_{max} - A_0)} + \frac{1}{K_{eq}(A_{max} - A_0)[M]^n} \quad (4)$$

where A_0 and A_x are the absorbance of the free FL dye and Ag NP/FL/CTAB complex, respectively. A_{max} is the saturated absorbance from the Ag NP/FL/CTAB mixed system. $[M]$ is the concentration of the CTAB solution. As FL is dianionic in the studied aqueous solution in the presence of Ag NPs and with CTAB being a monocation, the value of n may be taken as 2 considering 1:2 binding stoichiometry of the dye with CTAB.[49] The value of K_{eq} was obtained from the slope of the straight line plot of $1/(A_x - A_0)$ vs $1/[\text{CTAB}]^2$ as shown in Figure S6b and found to be 3.829×10^5 M^{-1} (Table 1). This high value of K_{eq} corresponds to the strong binding interaction between FL and CTAB in the 1:2 binding stoichiometry. The magnitude of K_{eq} is also related to the change in Gibbs free

Table 1. Equilibrium Constant (K_{eq}) and Gibbs Free Energy (ΔG) of Ag NP/FL/CTAB Complex[a]

K_{eq} (M^{-1})	R^2	ΔG (kJ mol^{-1})
3.829×10^5	0.932	−31.851

[a] R^2 is the corresponding correlation coefficient.

https://doi.org/10.1021/acs.langmuir.3c00204
Langmuir 2023, 39, 6713−6729

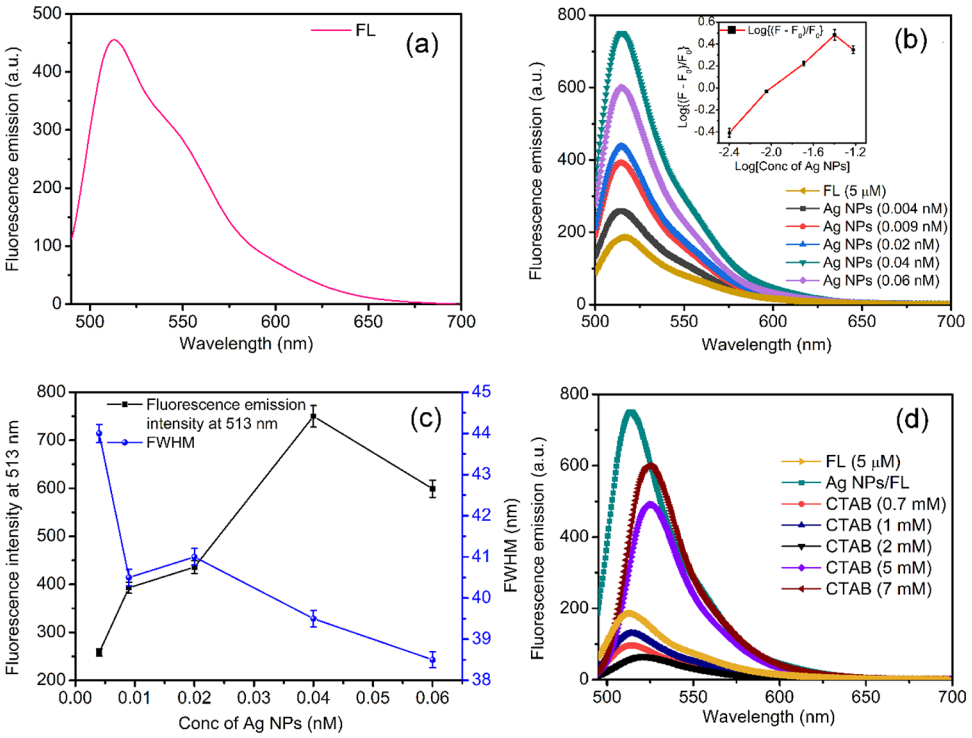

Figure 4. (a) Fluorescence spectrum of the FL aqueous solution (concentration of 10 μM). (b) Fluorescence spectra of the Ag NP/FL mixed solution for different concentrations of Ag NPs. (c) Plot of fluorescence intensity obtained from the Ag NP/FL mixed solution and FWHM vs different concentrations of Ag NPs. (d) Fluorescence spectra of the Ag NP/FL mixed solution in the presence of CTAB with different concentrations. The concentrations of Ag NPs and FL were 0.04 nM and 10 μM, respectively. Inset of panel b shows the plot of Log$\{(F - F_0)/F_0\}$ vs Log[Conc of Ag NPs].

energy (ΔG) during complexation between the species and is estimated using the equation[50] $\Delta G = -RT \ln K_{eq}$, where R is the universal gas constant and T is the absolute temperature. Both the values of K_{eq} and ΔG at ambient temperature (298 K) confirm the binding of FL with the micellar surface of CTAB in the aqueous solution.[47] Furthermore, the negative ΔG indicates that the interaction of CTAB with the Ag NP/FL system is spontaneous. In the presence of cationic micelles of CTAB, K_{eq} and ΔG represent a composite of electrostatic and hydrophobic interactions.[47]

Therefore, the present study reveals that the strong binding affinity between CTAB and dye molecules in the Ag NP/FL/CTAB mixed solution eventually favors the aggregations of dye species. However, the critical distance between the dye molecules toward the formation of dye aggregates is an important parameter and is generally known to be less than ~3.5 Å.[47] Various molecular association processes in different media are manifested as the shift (blue or red) of the absorption bands due to molecular exciton splitting when compared to their monomeric band.[51] Commonly, two types of molecular aggregates such as J-type for the band shift toward lower energy (red-shift) and H-type for the shift toward higher energy (blue-shift) are observed from the absorption spectrum of many organic molecules. In this study, for the Ag NP/FL/CTAB mixed system, the ~10 nm red-shift of the absorption band of dianionic dye species (as shown in Figure 2b,c) may be attributed to the formation of J-aggregates of dye molecules. To have a better understanding of the formation of J-aggregates, the Gaussian deconvolution of the experimental absorption spectra of Ag NP/FL/CTAB mixed solutions is performed. Each deconvoluted absorption spectrum shows three distinct bands with peaks centered at ~388, 472, and 500 nm, respectively, as presented in Figure S7.

The observed spectral changes may be understood with the help of the exciton coupling theory developed by Kasha et al.[51] considering the dipole−dipole interactions of the excitons of monomers. According to this theory, the geometrical structure of the aggregates is governed by the splitting of the excitonic energy levels of the monomers in the dimer and the angle between the transition dipole moments of the monomers (α) as well as the angle (θ) between the line joining the molecular centers and the transition moments of the monomers. This is schematically shown in Figure S8. Therefore, a perfect sandwich dimer (H-type) may be obtained where the molecules can stack one above the other so that their dipole moments are aligned in parallel planes with $\theta = 90°$ and $\alpha = 0°$. Generally, for H-dimers, the electronic transition from ground state to the most energetic excited state is allowed, but transition from ground state to the lowest energetic excited state is forbidden, and therefore, the H-dimer shows absorption bands at a higher energy side with respect to the monomeric absorption band. H-aggregates are generally nonfluorescent due to the very fast nonradiative deactivation to the lowest excited state. The other possibility is in-line head-to-tail or side-by-side arrangements (J-type) of the monomers, where the dipole moments are aligned in-line and coplanar with $\theta = 0°$ and $\alpha = 0°$. The J-dimer or aggregates can emit fluorescence due to the transition between the lowest excited state and the ground state resulting in a bathochromic shift (red-shift) of the monomer absorption spectrum. However, in general, the molecular chromophores can arrange themselves in aqueous solutions with any intermediate values of θ and α ($0° \le \theta \le 90°$ and $0° \le \alpha \le 90°$) resulting in the formation of

https://doi.org/10.1021/acs.langmuir.3c00204
Langmuir 2023, 39, 6713−6729

twisted type H- and J-aggregates. According to Martinez et al.,[52] the ratio between the area of H-band (A_H) and J-band (A_J) (obtained from the absorption intensities curve) is an indicative parameter for the type of dimer. For $A_H/A_J \geq 1.3$ ($\theta \geq 54.7°$),[52] the H-aggregate becomes prominent with diminished fluorescence emission intensity. For $A_H/A_J \leq 0.7$ ($\theta \leq 54.7°$),[52] the J-aggregate becomes prominent, which shows an additional band in the longer wavelength in the fluorescence spectrum of the fluorophore. The angle between monomeric units in the dimer (α in degree) can be determined using eq 5 from the exciton coupling theory:[51]

$$\alpha = 2\tan^{-1}\sqrt{(A_1/A_2)} \quad (5)$$

where A_1 and A_2 are the area of Gaussian bands corresponding to longer and shorter wavelengths, respectively. The values of θ for the J-dimer are determined with the help of the expression $\alpha + 2\theta = 180°$ by using the calculated value of α from eq 5. The value of θ is found to be ~42.5° (<54.7°), which also confirms the formation of the J-dimer of FL molecules in the mixed solution in the presence of CTAB. The complexation of FL dye molecules with CTAB micelle and the formation of their dimers or aggregates are schematically shown in Figure 3b.

Steady-State and Time-Resolved Fluorescence Emission Spectroscopic Studies. Although the UV−vis absorption spectroscopic study gives an indication of the formation of dimers or aggregates of FL dye molecules in the CTAB micellar medium in the presence of Ag NPs, the fluorescence spectroscopic technique is another important analytical approach for further understanding of the aggregated species of dye molecules from their excited-state molecular mechanism. Figure 4a shows the steady-state fluorescence emission spectrum of the FL aqueous solution (concentration of 10 μM). The experimental details of the spectroscopic characterization methods are discussed in the Supporting Information. An excitation wavelength of 474 nm was selected for all the steady-state fluorescence emission measurements. The FL dye shows a strong characteristic fluorescence emission band with a peak centered at ~513 nm accompanied with a prominent shoulder at ~545 nm. The emission band observed at ~513 nm may be due to the intrinsic fluorescence of FL monomeric monoanionic species.[27] The weak hump in the lower energy side of the spectrum is associated with the vibronic transition of the FL monomer.[20] However, in the presence of Ag NPs and CTAB, different factors such as the distribution and shape of NPs and separation between the metal surface and dye chromophores may affect the fluorescence of FL. Also, the surface morphology and LSPR of NPs play a crucial role in the observed SEF phenomenon. Figure 4b shows the fluorescence emission of FL (concentration of 10 μM) in the presence of Ag NPs with different concentrations, viz., 0.004, 0.009, 0.02, 0.04, and 0.06 nM. For Ag NP/FL mixed solutions, it is observed that the fluorescence intensity increases gradually with the increase in the concentration of Ag NPs and shows the maximum at 0.04 nM. Interestingly, on further increase in Ag NP concentrations in the mixed solution, the fluorescence intensity starts to decrease as shown in Figure 4b. The apparent binding constant (K_A) and number of binding sites (n_b) for the Ag NP/FL mixed solution are computed by using the linear Benesi−Hildebrand (BH) equation.[50]

$$\mathrm{Log}\left\{\frac{F - F_0}{F_0}\right\} = \mathrm{Log}(K_A) + n_b\mathrm{Log}[Q] \quad (6)$$

where F_0 and F are the steady-state fluorescence emission intensities of FL in the absence and presence of Ag NPs, respectively. [Q] is the concentration of Ag NPs. The values of K_A and n_b are obtained from the intercept and slope of the plot of Log{$(F - F_0)/F_0$} vs Log[Q] as shown in the inset of Figure 4b and are presented in Table 2. The Gibbs free energy (ΔG_0) for the Ag NP/FL mixed solution at 298 K is also calculated using the following expression:[50] $\Delta G_0 = -RT \ln K_A$, where R is the universal gas constant and T is the absolute temperature. The calculated value of ΔG_0 is presented in Table 2. The negative value of ΔG_0 as obtained from fluorescent data also indicates that the process of interactions is spontaneous.[48] The value of n_b reveals nearly one binding site of each FL molecule in the Ag NP/FL mixed solution. The interaction of dye molecules with cationic sites of CTAB is more favorable compared to that with Ag NPs as confirmed by the value of ΔG_0 because the dianionic form of FL in the mixed solution is responsible for their strong binding with CTAB molecules via electrostatic interaction.

Table 2. Values of the Apparent Binding Constant (K_A), Number of Binding Sites (n_b), and Gibbs Free Energy (ΔG_0) for the Ag NP/FL Mixed Solution[a]

K_A (M^{-1})	n_b	R^2	ΔG_0 (kJ mol^{-1})
50.889	0.871	0.993	−9.736

[a] R^2 is the corresponding correlation coefficient.

As stated earlier, when the concentration of Ag NPs is 0.06 nM in the dye solution, there is a decrease in fluorescence intensity as shown in Figure 4b. In fact, at such higher concentration (0.06 nM) of Ag NPs, the average internanoparticle distance might have decreased, resulting in the direct adsorption of some fraction of the dye molecules on the NP surface. This eventually causes the quenching of the overall fluorescence intensity of FL via some nonradiative decay. The distance-dependent enhancement and reduction of fluorescence of FL in the Ag NP colloidal aqueous medium are schematically illustrated in Figure 5. Similar quenching of fluorescence intensity due to the adsorption of organic fluorophores onto the NP surface has been studied by various researchers.[38,53] Figure 4c represents the plot of the fluorescence band intensity at ~513 nm as obtained from the Ag NP/FL mixed solution and full width at half-maximum (FWHM) vs different concentrations of Ag NPs. From this figure, it is clear that the maximum fluorescence enhancement occurs for the Ag NP/FL mixed solution with Ag NP concentration of 0.04 nM. On further increase in Ag NP concentrations, the reduced FWHM and the reduction in fluorescence intensity reveal an increase in the scattering of photons due to much closer association of NPs at their higher concentration in the mixed solution. However, from the steady-state fluorescence emission measurements of the Ag NP/FL mixed solution with Ag NPs (concentration of 0.04 nM), it is obvious that the interaction of NP surface plasmons with photoexcited dye molecules dominates over the scattering at some optimum internanoparticle distances in the mixed solution. Consequently, the overall fluorescence emission of the dye molecules was enhanced. Therefore, the corresponding fluorescence enhancement factor (FEF) at different wave-

https://doi.org/10.1021/acs.langmuir.3c00204
Langmuir 2023, 39, 6713−6729

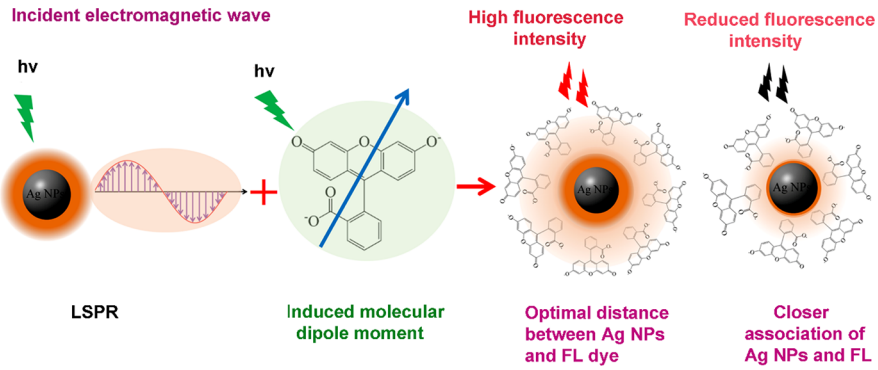

Figure 5. Schematic representation for the enhancement of fluorescence emission of FL dye in the presence of Ag NPs.

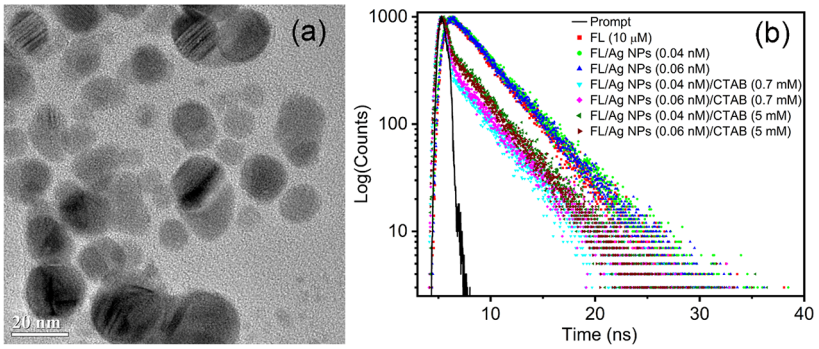

Figure 6. (a) TEM micrograph of the Ag NP/FL mixed sample. (b) Fluorescence decay plots (TCSPC) of the FL aqueous solution and Ag NP/FL mixed solution, respectively, in the absence and presence of CTAB at pre- and postmicellar concentrations.

lengths may be defined by the ratio of fluorescence emission intensity of the Ag NP/FL mixed solution for NP concentration of 0.04 nM to that of the pure FL aqueous solution (5 μM) and is shown in Figure S9. From this figure, it is clear that the highest FEF of ~4.108 is obtained at the wavelength of ~513 nm (the peak of fluorescence). However, FEF is decreased to ~3.282 for the Ag NP/FL mixed solution with NP concentration of 0.06 nM. Most possibly, the fluorescence enhancement occurred because of sufficient coupling between the electric field produced by the plasmonic oscillation of Ag NPs and the excited dipoles of the emitter in the vicinity of NPs in the mixed solution resulting in an increase in the radiative decay rate constant.[54] However, the relative orientation and the separation between the NPs are the two important factors toward the possibility of overall SEF. The decrease in FEF at a higher concentration of Ag NPs (i.e., 0.06 nM) is attributed to the decrease in spacing between the fluorophore (FL) and NPs as well as the increase in the number of nonradiative pathways of the emitter molecules located at very close proximity to the NPs. Fluorescence lifetime studies also support this observation as discussed later.

To support the observations from the UV−vis absorption and steady-state fluorescence emission spectroscopic study as already discussed above and also to have a direct visual evidence of the distribution of NPs in the presence of dye molecules, TEM study was performed. Figure 6a shows TEM micrograph of the Ag NP/FL mixed sample at an ambient condition. It is observed from this figure that Ag NPs formed closely spaced different-sized clusters or domains throughout the scanned sample surface. It is obvious that in the presence of FL dye, the NP medium is more viscous in the mixed solution. Interestingly, the NP distributions became more homogeneous, and the average size of NPs was increased to ~10.38 nm with SD of ~4.02 nm as is obtained from Figure S2b,c. However, the crystallinity of NPs almost remained unaltered, which is evidenced by the distinct diffraction rings observed in the SAED pattern of the Ag NP/FL mixed system (Figure S2d). This TEM study reveals that the relative separation between the dye molecules and NPs decreases because of the formation of cluster of Ag NPs in the mixed sample. As a result, the excited dipoles of dye molecules might have encountered the enhanced plasmonic field around the NPs, which is also manifested as the enhancement of fluorescence intensity of FL as shown in Figure 4b.

In general, this type of observed fluorescence enhancement is mainly attributed to two principal factors.[55] First is the increment of excitation rate due to the presence of local enhanced plasmonic field produced by the interaction between LSPR of NPs and incident EM radiation (photons). Second, the enhanced intrinsic radiative decay rate of fluorophore provides a higher quantum yield.[55] The excitation properties (f_E's) of spherical metal NPs having a size comparable to the wavelength of incident EM radiation may be represented by the combination of both scattering (f_S) and absorption (f_A) cross-section terms and are given by eq 7.[55]

$$f_E = f_A + f_S = k_1 \mathrm{Im}(\alpha) + \frac{k_1^4 |\alpha|^2}{6\pi} \quad (7)$$

where $\alpha = 4\pi r^3(\epsilon_m - \epsilon_1)/(\epsilon_m + 2\epsilon_1)$ is the polarizability of the sphere of radius r and ϵ_m and ϵ_1 are the dielectric constants of metal NPs and the first medium, respectively. $k_1 = 2\pi n_1/\lambda_0$ is the incident wave vector in the first medium. From the previous reports,[55] we may anticipate that the f_A term which increases as r^3, causes the fluorescence quenching, whereas the

https://doi.org/10.1021/acs.langmuir.3c00204
Langmuir 2023, 39, 6713−6729

Table 3. Time-Resolved Fluorescence Decay Parameters As Obtained from the Fitted Data of FL, Ag NP/FL, and Ag NP/FL/CTAB Solutions[a]

sample name		τ_1 (ns)	α_1	τ_2 (ns)	α_2	τ_{av} (ns)	χ^2
FL (10 μM)		1.9488	0.0550	3.6590	0.9449	3.565	1.078
FL/Ag NPs (0.04 nM)	CTAB (0 mM)	2.1976	0.0328	3.9411	0.9671	3.884	1.090
	CTAB (0.7 mM)	2.7330	0.5595	4.5780	0.4404	3.546	1.115
	CTAB (5 mM)	2.1648	0.1320	3.7203	0.8679	3.515	1.113
FL/Ag NPs (0.06 nM)	CTAB (0 mM)	1.9924	0.0775	3.8600	0.9224	3.715	1.154
	CTAB (0.7 mM)	2.2257	0.3904	4.2833	0.6095	3.479	1.120
	CTAB (5 mM)	1.2926	0.1379	3.6453	0.8620	3.321	1.002

[a]All the samples were excited at a wavelength of 450 nm. Decay data are fitted by two exponentials. χ^2 = fitting parameter; close to 1 means a good fit.

f_S term which increases as r^6, facilitates the fluorescence enhancement. According to the Mie theory,[56] for the small metal NPs (< 10 nm), f_A is the dominant term, resulting in the fluorescence quenching of the fluorophore in the vicinity of NPs. On the other hand, for large metal NPs or nanoclusters, f_S dominates over f_A, resulting in the SEF phenomenon of the fluorophores. Therefore, as the relative distance between NPs and dye molecules decreases with the increase in NP concentrations in the mixed solution, some fraction of the NPs can form clusters or larger-sized aggregated domains at the NP concentration of 0.04 nM as evidenced by the TEM study (Figure 6a). When two or more NPs come closer in the aqueous medium, the plasmonic fields may interfere constructively at an optimum average distance, leading to the enhancement of the resultant plasmonic electric field, which eventually facilitates the SEF from the organic fluorophore around the NPs.

As mentioned earlier, the fluorescence emission studies were also performed in the presence of the cationic surfactant CTAB to elucidate the effects of ionic guest species on the photophysical properties of the Ag NP/FL mixed system in an aqueous environment. The concentrations of the CTAB aqueous solution were chosen below and above its critical micellar concentration (CMC) (~0.92 mM).[57] Figure 4d represents the fluorescence emission spectra of the mixed solution of Ag NPs and FL in the absence and presence of CTAB of different concentrations. It is clearly observed that the fluorescence intensity is quenched with an almost unaltered peak position for the Ag NP/FL mixed solution with CTAB concentration of 0.7 mM compared to that in the absence of CTAB. This quenching may be attributed to the attachment of FL dye molecules with cationic CTAB molecules. However, on further increase in CTAB concentrations, the main fluorescence emission peak (~513 nm) gradually starts to shift toward the longer wavelength side and is observed at ~520 nm for both CTAB concentrations of 5 and 7 mM. This red-shift is an indication of the formation of dye aggregates due to their strong electrostatic interactions with cationic CTAB molecules. More precisely, at such higher concentrations, CTAB forms micelles that facilitate the closer association of FL molecules due to electrostatic interactions. As a result, dye aggregates are formed in the restricted geometry of CTAB molecules. Also, with the increase in CTAB concentration from the CMC, the number of such dye aggregates eventually increases, which is manifested as the enhancement of fluorescence intensity as shown in Figure 4d. The emergence of the higher wavelength emission peak in Figure 4d is due to the formation of J-type aggregates where the excited transition dipoles of monomer units are strongly coupled resulting in the delocalization of excited-state energies over neighboring monomers.[51,58]

However, to have a further understanding of the molecular species responsible for the observed fluorescence emission, fluorescence excitation spectra of the samples were recorded as shown in Figure S10. From this figure, it is observed that the excitation spectrum of pure FL with emission monitored at ~513 nm has a similarity with the UV−vis absorption spectrum of the FL aqueous solution. Also, the excitation spectrum of the Ag NP/FL mixed solution shows a nearly similar spectral profile except for some change in the intensity distribution of different peaks. However, most interestingly, the excitation spectra of the Ag NP/FL mixed solution in the presence of CTAB molecules are significantly red-shifted and broadened especially for higher CTAB concentrations. This peak broadening is generally attributed to the overlapping of the several vibrational levels associated with each electronic energy level of the dye molecules due to their closer association while interacting with cationic CTAB molecules in the aqueous solution. Therefore, the emission band observed at ~520 nm of FL in the presence of the CTAB solution corresponds to the formation of J-type aggregates (head-to-tail molecular stacking).

We have also studied the fluorescence emission spectra of the Ag NP/FL mixed solution in the presence of CTAB for another concentration of Ag NPs, i.e., 0.06 nM, in the same aqueous environment. However, similar spectral changes are observed except for the change in the intensity distribution of fluorescence emission peaks as shown in Figure S11. This observation reveals that dianionic FL has a much stronger interaction with cationic CTAB molecules even at higher concentrations of Ag NPs in the aqueous medium. More precisely, it can be concluded that most of the cationic binding sites are covered with anionic FL molecules in the mixed solution.

The time-resolved fluorescence emission spectroscopic studies were performed to comprehend the steady-state fluorescence spectroscopic results. The characterization method of this study is discussed in the Supporting Information. All the sample solutions were excited at a wavelength (λ_{ex}) of 450 nm, and the corresponding fluorescence emissions were monitored at a wavelength of maximum fluorescence intensity as obtained by steady-state measurements. The time-resolved fluorescence emission decay data of the FL dye solution (concentration of 10 μM) were recorded by using the time correlated single photon counting (TCSPC) method in the absence and presence of Ag NPs and CTAB. The fluorescence decay spectra as shown in Figure 6b and Figure S12 are well fitted by two exponentials according to

https://doi.org/10.1021/acs.langmuir.3c00204
Langmuir 2023, 39, 6713−6729

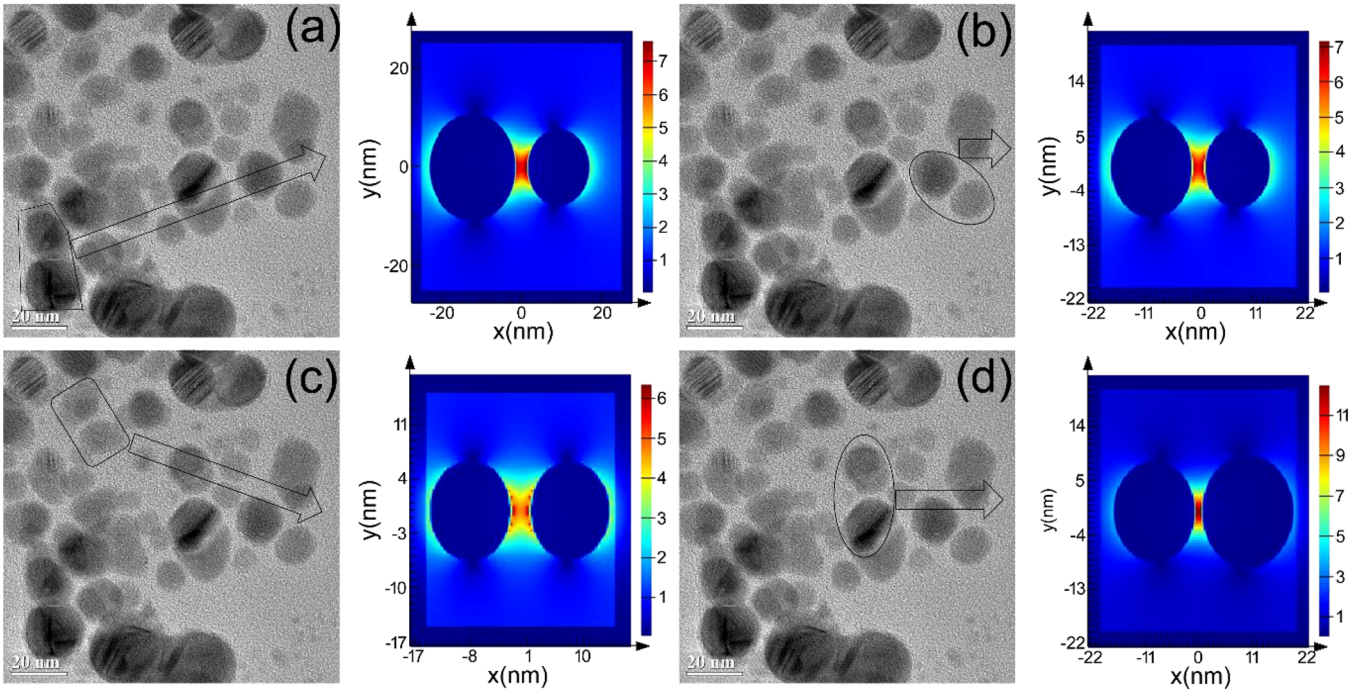

Figure 7. Distribution of the electric field around the hotspots as estimated by the 3D-FDTD simulation study for various interparticle separations: (a) ∼2.879 nm, (b) ∼2.575 nm, (c) ∼3.194 nm, and (d) ∼1.44 nm measured from the TEM image (Figure 6a) of the Ag NP/FL mixed sample. The polarizations of the incident light waves were considered along the *Z*-axis.

eq 8. The average fluorescence lifetimes (τ_{av}'s) of FL are determined by using eq 9[38] and are summarized in Table 3.

$$I(t) = \alpha_1 e^{-t/\tau_1} + \alpha_2 e^{-t/\tau_2} \quad (8)$$

$$\tau_{av} = \frac{\sum_i \alpha_i \tau_i}{\sum_i \alpha_i} \quad (9)$$

where τ_1 and τ_2 are the fluorescence lifetimes of the molecules with normalized pre-exponential factors of α_1 and α_2, respectively. The observed fluorescence lifetime (τ_{obs}) of FL and fluorescence intensity may be related by eq 10.[38]

$$\tau_{obs} = \frac{1}{K_{obs}} = \frac{1}{K_r + K_{nr} + K_{et}} \quad (10)$$

K_{obs} is the observed decay rate that is the inverse of τ_{obs}. K_{obs} includes the radiative decay rate (K_r), nonradiative decay rate (K_{nr}), and rate of energy transfer (K_{et}), if any. For a particular fluorophore in a specific microenvironment, both K_r and K_{nr} remain constant.[32] The τ_{av} of pure FL (10 μM) is calculated as ∼3.565 ns,[59] which is increased to ∼3.884 ns after addition of Ag NP dispersion (0.04 nM). This enhancement of τ_{av} might be due to the increase in excited-state energies of FL molecules due to the coupling of their oscillating dipoles with the nearby plasmonic electric field created by Ag NPs after photoexcitation.[60] Initially, with the increase in Ag NP concentration in the mixed solution, the extent of overlap of the augmented electric field around the NPs and the oscillating dipoles of FL dye after photoexcitation increased, resulting in the increase in the excited-state energy of dye molecules. Although the scattering of radiation increased with the initial increase in NP concentration (i.e., 0.04 nM), plasmonic overlap was predominant over the scattering, resulting in the observed fluorescence enhancement. The increase of both the lifetime components (i.e., τ_1 and τ_2) is also correlated with the different excited-state energies of dye species due to NP plasmonic contribution. It is relevant to mention that the size and shape of the plasmonic band of metal NPs play a crucial role in the SEF of the fluorophore around NPs.[61] The metal NPs with a sharp plasmon resonance band have better control over the scattering of the EM wave around the fluorophore in the vicinity of NPs. In this work, the as-synthesized Au NPs of diameter ∼8.71 nm show a well-defined sharp plasmonic band that can facilitate better control over scattering by the NPs in the medium.

However, most interestingly, on further increase of NP concentration (i.e., 0.06 nM), the value of τ_{av} of FL is decreased to ∼3.715 ns. This reduction of τ_{av} as compared to that of the Ag NP/FL mixed solution with NP concentration of 0.04 nM is due to the closer association of dye molecules and NPs in the ensemble. The observed change in τ_{av} at higher Ag NP concentration is also consistent with the observed fluorescence quenching (Figure 4b) and is possibly due to the reduction of relative distance between NPs and dye molecules as well as the sufficient coupling of the oscillating dipoles of the emitter and collective LSPR of NPs.[62] Lakowicz[63] reported that the quenching of fluorescence of organic fluorophore is usually observed when the molecules are at shorter distances (<5 nm) from the metal NP surface. Therefore, in our study, at such higher concentration of NPs (0.06 nM), some fraction of excited energy of FL dye is lost via a nonradiative energy transfer mechanism, mainly the surface energy transfer (SET) due to the close proximity of NPs and dye molecules. More precisely, the observed fluorescence quenching and hence the lifetime of FL dye at higher Ag NP concentration are a result of the interplay between the change in radiative deactivation rate (K_r) and the nonradiative SET.[64] Thus, K_{et} and K_{nr} in eq 10 play the dominant role in the reduction of observed fluorescence lifetime of FL for higher concentrations of NPs.

https://doi.org/10.1021/acs.langmuir.3c00204
Langmuir 2023, 39, 6713−6729

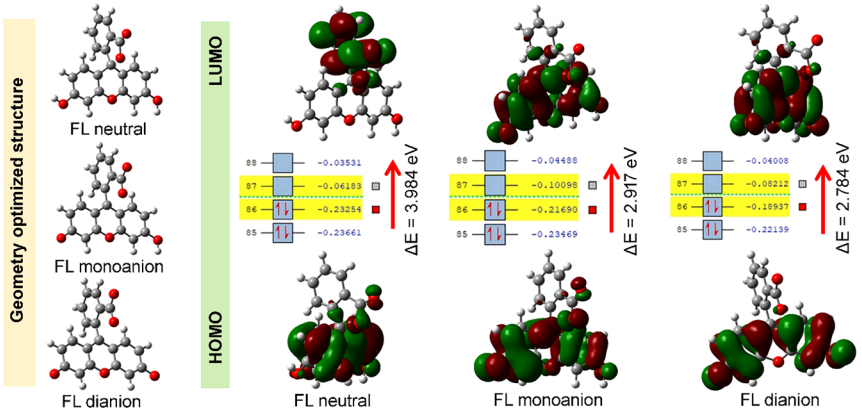

Figure 8. Geometry optimized structure and frontier molecular orbitals (HOMO and LUMO) associated with the electronic states of neutral and anionic species of FL dye molecules as obtained by using the B3LYP/6-31G and B3LYP/6-31 + G level of theory. The excitation energies (ΔE's) are calculated from the TD-DFT calculation using the same level of theory.

On the other hand, the τ_{av} for the Ag NP/FL mixed solution (with concentrations of 0.04 nM and 10 μM, respectively) in the presence of premicellar CTAB (0.7 mM) is found to be ∼3.546 ns, which is less compared to that in the absence of CTAB (∼3.884 ns), and this indicates the formation of different species of FL (J-aggregates).[58] Moreover, in the presence of postmicellar CTAB (5 mM), the further decrease of τ_{av} (i.e., ∼3.515 ns) corresponds to the presence of a large number of J-aggregates of FL with different molecular orientations in the aqueous medium. These observations should be correlated with the red-shift of the steady-state fluorescence emission spectra of Ag NP/FL in both pre- and postmicellar solutions of CTAB. A similar type of fluorescence lifetime results is also found in the case of the Ag NP/FL mixed solution at a higher NP concentration (i.e., 0.06 nM) with both pre- and postmicellar CTAB.

3D-FDTD Simulation. To establish a correlation between distance-dependent metal NP mediated SEF of FL dye and the spatial distribution of near-field EM wave around the plasmonic Ag NPs, 3D-FDTD simulations studies were performed. The strong LSPR band of metallic NPs can generate evanescent waves that may give spatial frequency information during interaction with different guest fluorophores.[65] The strongly localized near-field distribution around the NPs interacts with plasmonic oscillation of nearby NPs, leading to the confinement of a large amount of EM field, which is responsible for the creation of various hotspots in the vicinity of NPs. Such hotspots play a pivotal role toward the SEF of organic molecules placed in the assembly of NPs or nanoclusters.[65] The TEM images of pure Ag NPs (Figure 1b) and the Ag NP/FL mixed sample (Figure 6a) show some changes of morphological features of the NPs. It is observed that various aggregated domains or clusters of NPs are formed as a result of their interaction with dye molecules in the aqueous medium. These clusters or aggregated domains of NPs eventually favor the creation of various hotspot geometries due to the overlapping of LSPR modes of NPs resulting in the confinement and augmentation of the localized EM field on photoexcitation. Figure 7a−d presents the different hotspot geometries corresponding to the spatial distributions of the electric field as estimated theoretically via the 3D-FDTD simulation approach considering various interparticle separations measured from the TEM image (Figure 6a) of the Ag NP/FL mixed sample. The prominent hotspots (red color) are generated from the simple heterodimeric nearly spherical aggregates of Ag NPs. It is clear from this study that these simple heterodimeric spherical aggregates of NPs are therefore effective to create various hotspots. Recently, some researchers[66] also suggested that simple dimeric aggregations are more favorable in the creation of such hotspots that are responsible for SEF of organic fluorophores around the plasmonic metal NPs. The literature also reveals that the LSPR of metal NPs is strongly coupled by photon tunneling through the interparticle gap of less than ∼2.5 times the short-axis length of the NPs resulting in a strong EM field around the NPs.[67] However, the increase in internanoparticle separation reduces such plasmonic coupling. The coupling strength between the NPs may be represented by eq 11.[68]

$$E \propto e^{-ar}/\sqrt{r} \tag{11}$$

where a and r are the propagation length of the surface mode and separation between the NPs, respectively. This relation clearly indicates that the coupling between NPs decays exponentially with the increase in NP separation for a constant value of a (10 μm).[68] The hottest among the hotspots is identified and is shown in Figure 7d. The estimated magnitude of the hottest electric field is ∼12.2 V m^{-1}, which is distributed over a distance of ∼6 nm with interparticle separation of ∼1.44 nm. Thus, this study reveals that the simple heterodimeric nanostructure is favorable for creating such hottest geometry producing a strong electric field. By considering the solvent accessible surface area (SASA) of FL dye molecules as ∼371 Å^2, it is evident that the area of the simulated hotspot can accommodate more than two guest dye molecules that can participate in SEF.

According to the plane wave approximation and by considering the EM near-field distribution of LSPR of Ag NPs, the hottest among the ensemble of hotspots with a simulated electric field magnitude of ∼12.2 Vm^{-1} is attributed to an FEF of ∼4.108. Therefore, the enhanced electric fields produced by various hotspot geometries eventually may interact constructively with the oscillating dipoles of dye molecules, thereby showing the enhanced fluorescence intensity that is reflected in the steady-state emission measurements.

DFT Study. DFT is an important theoretical approach for studying the electronic structure and molecular mechanism

https://doi.org/10.1021/acs.langmuir.3c00204
Langmuir 2023, 39, 6713−6729

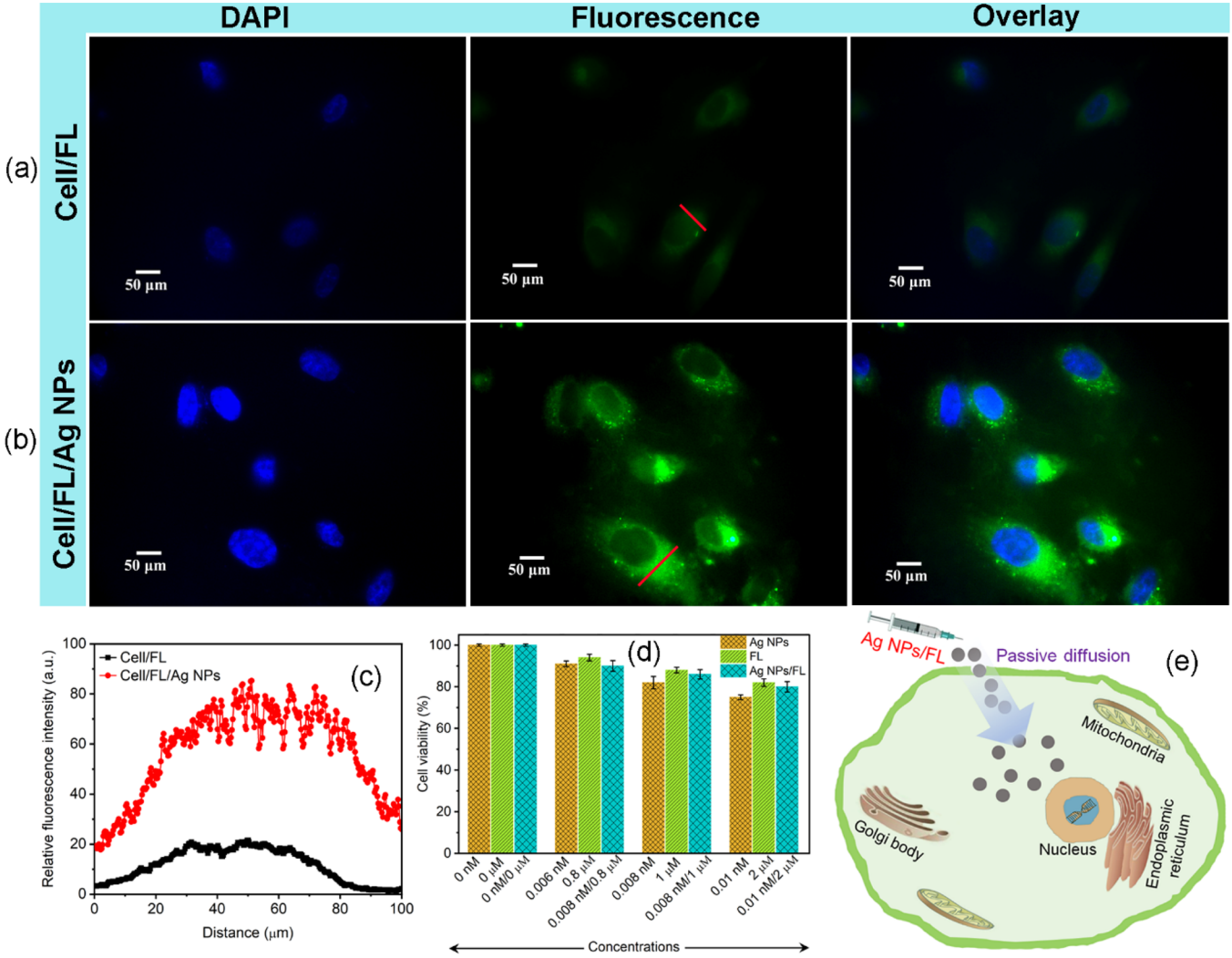

Figure 9. Fluorescence microscopic images of human lung fibroblast cells (WI 38 cell line) after treatment with (a) FL and (b) Ag NP/FL mixed sample. Concentrations of Ag NPs and FL dye were 0.006 nM and 0.8 μM, respectively. (c) Intensity profiles obtained from images a and b along the line (red color). (d) Cell viability study for 3 h of incubation as obtained by the MTT assay method. Mixed solutions of Ag NPs and FL were prepared in a 1:1 volume ratio. (e) Schematic presentation of the penetration of the Ag NP/FL mixed system through the cell membrane.

responsible for various photophysical processes of molecular systems in different microenvironments. Figure 8 shows the geometry optimized structure of different species of FL dye in a solvent (water) background using the IEFPCM model. The neutral and anionic forms of FL dye were optimized by the B3LYP/6-31G and B3LYP/6-31 + G level of theory, respectively, using the Gaussian 09 suit of software.[33] We also performed TD-DFT calculation using the same level of theory as was used for geometry optimization. The HOMO−LUMO energy differences or the excitation energies between the singlet states for neutral, monoanion, and dianion forms are ∼3.984, ∼2.917, and ∼2.784 eV, respectively. The theoretical study also reveals that the main strong characteristic transition of FL dye is attributed to the $\pi-\pi^*$ transition of the xanthene moiety.[69] From this study, it is predicted that the excitation energy is the minimum for anionic dye species, and the result is consistent with the experimental UV−vis absorption study of the dye aqueous solution. The resultant transition dipole moments for the ground state to the first excited state transition of neutral, monoanionic, and dianionic forms are ∼0.12, ∼2.503, and ∼3.483 D, respectively. The difference in transition dipole moments as estimated from TD-DFT calculation is manifested as the observed spectral changes for different molecular species of FL dye. Therefore, the well converging nature of this theoretical study signifies various important information on the electronic structures and molecular mechanism involved in their ground electronic states.

Human Cell Imaging. Cellular imaging via the fluorescence method is an excellent and conventional choice to assess various cellular phenotypic changes as well as the role of a particular agent in the in vitro study of diseases. Also, the fluorescence imaging microscopic method has emerged in the biomedical research for routine studies to realize various biophysical and biochemical processes in the living cells.[70] However, this elegant method requires an optimum resolution to image intracellular and extracellular medium of living cells. The use of traditional organic fluorescence dyes in fluorescence imaging microscopy is limited because of their low quantum yield, small Stokes shift, less stability in the excited state, and inefficiency in suppressing the autofluorescence from various intracellular components during cellular imaging.[71] Additionally, because of the hydrophilic nature of most of the traditional organic dyes, they are normally inefficient to

https://doi.org/10.1021/acs.langmuir.3c00204
Langmuir 2023, 39, 6713−6729

penetrate through the cell membrane at very low concentrations, and an increase in their concentration can induce moderate to high cytotoxicity. To circumvent these issues in cellular imaging, it is essential to tailor the spectral properties and related photophysical behaviors of those organic fluoroprobes for their suitability with higher resolution and better optical contrast. Several studies on metal−fluorophore interactions in the nanoscale reveal the fluorescence emission enhancement of organic fluorophores in close proximity to the metal surface, thereby creating new opportunities of applications of nanophotonics for biomedical interest.[72] In this regard, the plasmonic NPs such as Au NPs, Ag NPs, Cu NPs, etc., are promising candidates toward the fluorescence enhancement of organic fluoroprobes through coupling of LSPR and oscillating dipoles of the emitters.[73] In this work, we have systematically studied the improvement of fluorescence signal and other related photophysical parameters of biologically relevant water-soluble organic dye FL in aqueous media. As most of the in vitro studies of cell and tissue culture are performed in aqueous media, it is therefore expected to consider the combination of these metallic nanostructures (Ag NPs) and FL with enhanced fluorescence signal as a promising approach for cellular imaging applications. In this study, we performed the fluorescence imaging of healthy human lung fibroblast cells (WI 38 cell line) as shown in Figure 9a,b after treatment with both FL dye and Ag NP/FL mixed solutions for an incubation period of 3 h. From these figures, it is observed that Ag NPs and FL dye successfully entered into the cytoplasmic region of the cell but did not penetrate to the nucleus as a distinct blue color region is clearly differentiated. The blue color emission from the nucleus is due to its selective interaction with DAPI as used in this experiment.[73] DAPI is basically used to selectively identify the nucleus in the intracellular region. The fluorescence images reveal that both FL and Ag NP/FL mixed systems seem to have no or significant interaction with the nucleus but only emit a signal from the entire cytoplasmic domain in the cell. FL has a dianionic form in physiological pH.[45] It is relevant to mention that charged hydrophilic compounds are generally inefficient to penetrate through the cell membrane via any specific mechanism due to the hydrophobicity and ionic nature of the cell membrane. We tested the FL dye solution with a very low concentration (as a low concentration is always preferable to avoid any significant cytotoxicity) in the cell culture medium but did not obtain any appreciable fluorescence signal (figure not shown) during cellular imaging. However, after slightly increasing the concentration of the dye solution in the culture medium and allowing some incubation time, the dye molecules successfully entered into the cell as evidenced by the fluorescence image (Figure 9a). This cellular internalization of these small polar molecules might have occurred via some diffusion process.[74] It is also observed from the figure that when the cells were exposed to FL dye only, they show a low green fluorescence emission from the intracellular cytoplasmic region. However, most interestingly, after exposure to the Ag NP/FL mixed solution, the fluorescence image of the cells gives an intense green fluorescence emission as shown in Figure 9b. The relative fluorescence intensity for the FL and Ag NP/FL mixed system along the line section (Figure 9a,b) as a function of distance is shown in Figure 9c. From this figure, it is also evident that the fluorescence intensity is much higher for the Ag NP/FL system compared to when only FL entered in the cell. Also, the metal NP/dye based probe system is distributed throughout the cytoplasmic region showing a well-defined spatial boundary with the nucleus (blue color region). This study reveals that, after addition of Ag NPs, dye molecules exhibit similar metal enhanced fluorescence of FL in the cytoplasmic region as was also observed previously in the aqueous medium without a cell. Therefore, the plasmonic metal nanostructures efficiently improve the resolution of the cellular image with much better contrast.

However, good cellular imaging requires cell viability and proper biocompatibility of the fluorescent probe against the cells to be studied. In this regard, to know the cell viability with the Ag NP/FL mixed system, various amounts of Ag NPs, FL, and Ag NP/FL were added to the culture medium of human lung fibroblast cells separately and incubated for 3 h. The cellular viability was then determined by the MTT assay method as already described in the Experimental Section. The 3 h incubation time was chosen as the fluorescence imaging was performed after the same incubation time. From MTT assay results shown in Figure 9d, it is observed that more than 90% cells were alive after being treated with the Ag NP/FL mixed solution (volume of 150 μL). These results confirm the viability of the proposed Ag NP/dye based probe system for efficient cellular imaging. The penetration of the Ag NP/FL mixed system into the cell is schematically shown in Figure 9e. However, the cellular entry of Ag NPs can vary based on the type of the cell. Because of the nanoscale size of Ag NPs, the internalization of Ag NPs could involve some nonspecific mechanism if individual NPs can diffuse through the cell membrane along with the dye molecules.[75,76] The literature suggests that the uptake kinetics and intracellular localization of the NPs may depend on the size and surface characteristics of NPs, ability to form aggregates, etc.[24] Although the amphiphilicity of the constituent phospholipids of the bilayer assemblies of the cell membrane may be an important factor to make the cell membrane an efficient selective barrier, a balanced hydrophilicity/hydrophilicity of the membrane permits the penetration of such metal NP/dye system into the cell via the diffusion process.[77]

CONCLUSIONS

In conclusion, this study demonstrates the surface enhanced fluorescence of organic dye FL while interacting with colloidal Ag NPs in an aqueous solution. This enhancement of fluorescence of FL dye due to Ag NPs is also observed in fluorescence images of human lung fibroblast cells (WI 38 cell line) after being treated with the Ag NP/FL mixed aqueous solution. The FL dye forms its dianionic species in the aqueous solution containing Ag NPs as confirmed by UV−vis absorption and steady-state and time-resolved fluorescence emission spectroscopic studies. The higher values of association constants and Gibbs free energies of Ag NP/FL/CTAB and Ag NP/FL mixed ensembles as estimated from UV−vis absorption and fluorescence emission spectroscopic results give a conclusive evidence for the greater extent of interaction between FL and CTAB in their mixed solution when compared to that in the case of the Ag NP/FL system. The strong electrostatic interactions between cationic CTAB and dianionic FL dye facilitate the formation of J-type molecular dimer or aggregates of FL in the presence of Ag NPs as evidenced by UV−vis absorption and fluorescence spectroscopic results. The J-type aggregates of FL dye are manifested as the red-shift of the absorption band when compared to their monomer absorption band. The 3D-FDTD

https://doi.org/10.1021/acs.langmuir.3c00204
Langmuir 2023, 39, 6713−6729

theoretical simulation study reveals the formation of various hotspots due to the plasmonic overlapping of the local electric field between the neighboring NPs. The interaction of the augmented local electric field generated by Ag NPs with excited dipoles of dye molecules is responsible for the overall fluorescence enhancement that also depends on the internanoparticle separation. More precisely, this fluorescence enhancement depends on the concentration of Ag NPs in the mixed ensemble. The DFT study reveals the information about the electronic energy levels and the transition dipole moments of the various forms of FL molecules in the aqueous medium. The fluorescence microscopic image of human lung fibroblast cell shows a much stronger green emission from the entire cytoplasmic region of the cells after being treated with the Ag NP/FL mixed sample for 3 h of incubation when compared with cells treated with FL dye only. The penetration of the FL dye and Ag NP/FL mixed system into the intracellular region through the cell membrane occurred possibly because of some nonspecific diffusion mechanism under the balanced hydrophilic/hydrophilic condition of the cell membrane. More than 90% of the cells were viable after exposure with the Ag NP/FL mixed solution as confirmed by the cytotoxicity study through the MTT assay method. The remarkable brightness obtained in the cellular medium mediated by Ag NPs via metal surface enhanced fluorescence ensures their promising and continued importance in biomedical applications.

■ ASSOCIATED CONTENT

Supporting Information

The Supporting Information is available free of charge at https://pubs.acs.org/doi/10.1021/acs.langmuir.3c00204.

Materials; synthesis of Ag NPs; preparation of mixed samples; characterization techniques; DLS and zeta potential spectra; TEM study; chemical structures of different species of FL; schematic for the formation of FL anionic species; Gaussian deconvolution spectra of Ag NP/FL solutions; UV−vis absorption spectra of FL/CTAB solution; plot of the modified Benesi−Hildebrand equation; Gaussian deconvolution spectra of the Ag NP/FL/CTAB solution; schematics of H- and J-dimer; fluorescence enhancement factor vs wavelength plot; excitation spectra; fluorescence spectra of Ag NP/FL/CTAB solution; time-resolved fluorescence spectra; and spectroscopic parameters (Table S1) (PDF)

■ AUTHOR INFORMATION

Corresponding Author

Pabitra Kumar Paul − *Department of Physics, Jadavpur University, Kolkata 700032, India;* orcid.org/0000-0002-3490-525X; Phone: +91-9477631142; Email: pabitra_tu@yahoo.co.in, pabitrak.pal@jadavpuruniversity.in

Authors

Pradip Maiti − *Department of Physics, Jadavpur University, Kolkata 700032, India;* orcid.org/0000-0001-6879-591X

Swarupa Sarkar − *Department of Life Science & Biotechnology, Jadavpur University, Kolkata 700032, India*

Tanmoy Singha − *Department of Physics, Jadavpur University, Kolkata 700032, India;* orcid.org/0000-0002-4683-6204

Sannak Dutta Roy − *Department of Physics, Sammilani Mahavidyalaya, Kolkata 700075, India*

Mrityunjoy Mahato − *Physics Division, Department of Basic Sciences & Social Science, North-Eastern Hill University, Shillong 793022 Meghalaya, India;* orcid.org/0000-0002-6815-2399

Parimal Karmakar − *Department of Life Science & Biotechnology, Jadavpur University, Kolkata 700032, India*

Sharmistha Paul − *West Bengal State Council of Science and Technology, Department of Science and Technology and Biotechnology, Kolkata 700064, India*

Complete contact information is available at: https://pubs.acs.org/10.1021/acs.langmuir.3c00204

Notes

The authors declare no competing financial interest.

■ ACKNOWLEDGMENTS

P.M. wishes to thank Jadavpur University and Rashtriya Uchchatar Shiksha Abhiyan (RUSA) 2.0 (Ref. No. R-11/604/19) for providing excellent infrastructural and financial support to perform the experimental studies. P.K.P., P.M., and S.P. are grateful to the West Bengal State Council of Science and Technology, Govt. of West Bengal, for financial assistance (Ref. No. 493/WBSCST/F/0545/15(Pt-I) to perform this work. P.K.P. is also thankful to SERB-DST, Govt. of India, for financial assistance (Ref. No. SB/EMEQ-142/2014).

■ REFERENCES

(1) Wang, F.; Yue, X.; Ding, Q.; Lin, H.; Xu, C.; Li, S. Chiral inorganic nanomaterials for biological applications. *Nanoscale* **2023**, *15*, 2541−2552.

(2) Ratre, P.; Jain, B.; Kumari, R.; Thareja, S.; Tiwari, R.; Srivastava, R. K.; Goryacheva, I. Y.; Mishra, P. K. Bioanalytical Applications of Graphene Quantum Dots for Circulating Cell-Free Nucleic Acids: A Review. *ACS Omega* **2022**, *7*, 39586−39602.

(3) Ishikawa-Ankerhold, H. C.; Ankerhold, R.; Drummen, G. P. C. Advanced Fluorescence Microscopy Techniques−FRAP, FLIP, FLAP, FRET and FLIM. *Molecules* **2012**, *17*, 4047−4132.

(4) Hossain, M. K.; Mukhaimer, A. W.; Al-Jabari, M. Fabrication and characterizations of arbitrary-shaped silver nanoparticles for surface-enhanced fluorescence microscopy. *J. Nanopart. Res.* **2021**, *23*, 89.

(5) Jeong, Y.; Kook, Y. M.; Lee, K.; Koh, W. G. Metal enhanced fluorescence (MEF) for biosensors: General approaches and a review of recent developments. *Biosens. Bioelectron.* **2018**, *111*, 102−116.

(6) Sandhu, S.; Kydd, L. N.; Jaworski, J. Luminescent Probe Based Techniques for Hypoxia Imaging. *J. Nanomed. Res.* **2017**, *6*, No. 00160.

(7) Zhu, X.; Su, Q.; Feng, W.; Li, F. Anti-Stokes shift luminescent materials for bio-applications. *Chem. Soc. Rev.* **2017**, *46*, 1025−1039.

(8) Dutta Choudhury, S.; Badugu, R.; Lakowicz, J. R. Directing Fluorescence with Plasmonic and Photonic Structures. *Acc. Chem. Res.* **2015**, *48*, 2171−2180.

(9) Karlsson, H. L.; Toprak, M. S.; Fadeel, B. Toxicity of metal and metal oxide nanoparticles. Editor(s): Gunnar F., Nordberg; Max, Costa *Handbook on the Toxicology of Metals* (5th Ed.). Academic Press. 2022, 87−126.

(10) Sajida, M.; Płotka-Wasylka, J. Nanoparticles: Synthesis, characteristics, and applications in analytical and other sciences. *Microchem. J.* **2020**, *154*, No. 104623.

(11) Han, J.; Won, M.; Kim, J. H.; Jung, E.; Min, K.; Jangili, P.; Kim, J. S. Cancer stem cell-targeted bio-imaging and chemotherapeutic perspective. *Chem. Soc. Rev.* **2020**, *49*, 7856−7878.

(12) Devasenathipathy, R.; Wang, J. Z.; Xiao, Y. H.; Rani, K. K.; Lin, J. D.; Zhang, Y. M.; Zhan, C.; Zhou, J. Z.; Wu, D. Y.; Tian, Z. Q. Plasmonic Photoelectrochemical Coupling Reactions of para-Amino-

benzoic Acid on Nanostructured Gold Electrodes. *J. Am. Chem. Soc.* **2022**, *144*, 3821−3832.
(13) Geddes, C. D. *Reviews in Plasmonics 2017*; Springer, 2018.
(14) Bhaskar, S.; Rai, A.; Ganesh, K. M.; Reddy, R.; Reddy, N.; Ramamurthy, S. S. Sericin-Based Bio-Inspired Nano-Engineering of Heterometallic AgAu Nanocubes for Attomolar Mefenamic Acid Sensing in the Mobile Phone-Based Surface Plasmon-Coupled Interface. *Langmuir* **2022**, *38*, 12035−12049.
(15) Drexhage, K. H. Interaction of Light with Monomolecular Dye Layers, Editor(s): E., Wolf, *Progress in Optics*; Elsevier, 1974, *12*, 163−232, DOI: 10.1016/S0079-6638(08)70266-X.
(16) Subramanyam, P.; Meena, B.; Biju, V.; Misawa, V.; Subrahmanyam, C. Emerging materials for plasmon-assisted photoelectrochemical water splitting. *J. Photochem. Photobiol., C* **2022**, *51*, No. 100472.
(17) Bhaskar, S.; Moronshing, M.; Srinivasan, V.; Badiya, P. K.; Subramaniam, C.; Ramamurthy, S. S. Silver Soret Nanoparticles for Femtomolar Sensing of Glutathione in a Surface Plasmon-Coupled Emission Platform. *ACS Appl. Nano Mater.* **2020**, *3*, 4329−4341.
(18) Bhaskar, S.; Kowshik, N. C. S. S.; Chandran, S. P.; Ramamurthy, S. S. Femtomolar Detection of Spermidine Using Au Decorated SiO_2 Nanohybrid on Plasmon-Coupled Extended Cavity Nanointerface: A Smartphone-Based Fluorescence Dequenching Approach. *Langmuir* **2020**, *36*, 2865−2876.
(19) Seaberg, J.; Montazerian, H.; Hossen, M. N.; Bhattacharya, R.; Khademhosseini, A.; Mukherjee, P. Hybrid Nanosystems for Biomedical Applications. *ACS Nano* **2021**, *15*, 2099−2142.
(20) Bhaskar, S.; Das, P.; Srinivasan, V.; Shivakiran Bhaktha, B. N.; Ramamurthy, S. S. Bloch Surface Waves and Internal Optical Modes-Driven Photonic Crystal-Coupled Emission Platform for Femtomolar Detection of Aluminum Ions. *J. Phys. Chem. C* **2020**, *124*, 7341−7352.
(21) Dulkeith, E.; Morteani, A. C.; Niedereichholz, T.; Klar, T. A.; Feldmann, J.; Levi, S. A.; van Veggel, F. C. J. M.; Reinhoudt, D. N.; Möller, M.; Gittins, D. I. Fluorescence Quenching of Dye Molecules near Gold Nanoparticles: Radiative and Nonradiative Effects. *Phys. Rev. Lett.* **2002**, *89*, No. 203002.
(22) Momenbeitollahi, N.; van der Zalm, J.; Chen, A.; Li, H. Entrapping gold nanoparticles in membranes for simple-to-use enhanced fluorescence detection of proteins. *Anal. Chim. Acta* **2022**, *1195*, No. 339443.
(23) Yin, N.; Liu, Y.; Liu, L.; Lei, J.; Jiang, T.; Wang, H.; Zhu, L.; Xu, X. Fluorescence enhancement of $Ru(bpy)_3^{2+}$ by core-shell $Ag@SiO_2$ nanocomposites. *J. Alloys Compd.* **2013**, *581*, 6−10.
(24) Medici, S.; Peana, M.; Nurchi, V. M.; Zoroddu, M. A. Medical Uses of Silver: History, Myths, and Scientific Evidence. *J. Med. Chem.* **2019**, *62*, 5923−5943.
(25) Jose, D. A.; Sakla, R.; Sharma, N.; Gadiyaram, S.; Kaushik, R.; Ghosh, A. Sensing and Bioimaging of the Gaseous Signaling Molecule Hydrogen Sulfide by Near-Infrared Fluorescent Probes. *ACS Sens.* **2020**, *5*, 3365−3391.
(26) De Sá, I. C.; Oliveira Silva, P. M.; Nossol, E.; Borges, P. H. S.; Lepri, F. G.; Semaan, F. S.; Dornellas, R. M.; Pacheco, W. F. Modified dry bean pod waste (Phaseolus vulgaris) as a biosorbent for fluorescein removal from aqueous media: Batch and fixed bed studies. *J. Hazard. Mater.* **2022**, *424*, No. 127723.
(27) Anselmo, S.; De Luca, G.; Ferrara, V.; Pignataro, B.; Sancataldo, G.; Vetri, V. Insight into mechanisms of creatinine optical sensing using fluorescein-gold complex. *Methods Appl. Fluoresc.* **2022**, *10*, No. 045003.
(28) Bakir, E. M.; Sayed, A. R.; Abd El-Lateef, H. M. Colorimetric detection of Hg^{2+} ion using fluorescein/thiourea sensor as a receptor in aqueous medium. *J. Photochem. Photobiol., A* **2022**, *422*, No. 113569.
(29) Sjöback, R.; Nygren, J.; Kubista, M. Absorption and fluorescence properties of fluorescein. *Spectrochim. Acta, Part A* **1995**, *51*, L7−L21.
(30) Zare, I.; Chevrier, D. M.; Rius, A. C.; Moradi, N.; Xianyu, Y.; Ghosh, S.; Alfonso, L. T.; Tian, Y.; Haghighi, A. S.; Mukherjee, M.; Fan, K.; Hamblin, M. R. Protein-protected metal nanoclusters as diagnostic and therapeutic platforms for biomedical applications. *Mater. Today*, 2021, DOI: 10.1016/j.mattod.2020.10.027.
(31) Zhang, X.; Zhang, X.; Tao, L.; Chi, Z.; Xu, J.; Wei, Y. Aggregation induced emission-based fluorescent nanoparticles: fabrication methodologies and biomedical applications. *J. Mater. Chem. B* **2014**, *2*, 4398−4414.
(32) Mo, Y. K.; Kankavi, O.; Masci, P. P.; Mellick, G. D.; Whitehouse, M. W.; Boyle, G. M.; Parsons, P. G.; Roberts, M. S.; Cross, S. E. Surfactant Protein Expression in Human Skin: Evidence and Implications. *J. Invest. Dermatol.* **2007**, *127*, 381−386.
(33) Frisch, M. J.; Trucks, G. W.; Schiegel, H. B.; Scuseria, G. E.; Robb, M. A.; Cheeseman, J. R.; Montgomery, Jr., J. A.; Vreven, T.; Kudin, K. N.; Burant, J. C.et al. *Gaussian 09*, Gaussian, Inc.: Pittsburgh, PA, 2009.
(34) Casalini, T.; Salvalaglio, M.; Perale, G.; Masi, M.; Cavallotti, C. Diffusion and Aggregation of Sodium Fluorescein in Aqueous Solutions. *J. Phys. Chem. B* **2011**, *115*, 12896−12904.
(35) Dennington, R.; Keith, T.; Millam, J. *GaussView 6.0.16*; Semichem Inc.: Shawnee Mission, KS, 2018.
(36) https://www.lumerical.com/tcad-products/fdtd/
(37) Chen, M.; Du, B.; Wang, Q.; Zhang, J.; Zhu, X.; Lin, Z.; Dong, Y.; Fu, F. F.; Yu, T. Tuning the aggregation of silver nanoparticles with carbon dots for the surface-enhanced Raman scattering application. *Carbon* **2021**, *185*, 442−448.
(38) Maiti, P.; Singha, T.; Chakraborty, U.; Dutta Roy, S.; Karmakar, P.; Dey, B.; Hussain, S. A.; Paul, S.; Paul, P. K. Selective and sensitive detection of L-Cysteine via fluorometric assay using gold nanoparticles and Rhodamine B in aqueous medium. *Mater. Chem. Phys.* **2019**, *234*, 158−167.
(39) Koch, A. H. R.; Morsbach, S.; Bereau, T.; Lévêque, G.; Butt, H.-J.; Deserno, M.; Landfester, K.; Fytas, G. Probing Nanoparticle/Membrane Interactions by Combining Amphiphilic Diblock Copolymer Assembly and Plasmonics. *J. Phys. Chem. B* **2020**, *124*, 742−750.
(40) Söderlund, J.; Kiss, L. B.; Niklasson, G. A.; Granqvist, C. G. Lognormal Size Distributions in Particle Growth Processes without Coagulation. *Phys. Rev. Lett.* **1998**, *80*, 2386.
(41) Jiang, C.; Zhang, H.; Li, P.; Zhan, X.; Liu, Z.; Wang, L.; Mao, B.; Li, Q.; Wen, Z.; Peng, Z.; Chen, S.; Liu, Z. A Highly Stable All-Solid-State $Na-O_2/H_2O$ Battery with Low Overpotential Based on Sodium Hydroxide. *Adv. Funct. Mater.* **2022**, *32*, 2202518.
(42) Salimi, R.; Sabbagh Alvani, A. A.; Sameie, H.; Poelman, D.; Rosei, F. Designing 1D Plasmonic $Ag/CuWO_4$ Nanocomposite for Enhancing Visible-Light Photoelectrochemical Performance. *J. Electrochem. Soc.* **2022**, *169*, No. 086503.
(43) Raza, S.; Ansari, A.; Siddiqui, N. N.; Ibrahim, F.; Abro, M. I.; Aman, A. Biosynthesis of silver nanoparticles for the fabrication of noncytotoxic and antibacterial metallic polymer based nanocomposite system. *Sci. Rep.* **2021**, *11*, 10500.
(44) Paramelle, D.; Sadovoy, A.; Gorelik, S.; Free, P.; Hobleya, J.; Fernig, D. G. A rapid method to estimate the concentration of citrate capped silver nanoparticles from UV-visible light spectra. *Analyst* **2014**, *139*, 4855−4861.
(45) Martin, M. M.; Lindqvist, L. The pH dependence of fluorescein fluorescence. *J. Lumin.* **1975**, *10*, 381−390.
(46) Singha, D.; Sahu, D. K.; Sahu, K. Coupling of Molecular Transition with the Surface Plasmon Resonance of Silver Nanoparticles inside the Restricted Environment of Reverse Micelles. *ACS Omega* **2017**, *2*, 5494−5503.
(47) Debnath, C.; Saha, M.; Hussain, S. A.; Bhattacharjee, D. Micellar effect of surfactant on the aggregation pattern of a fluorescent dye in ultra-thin film. *J. Photochem. Photobiol., C* **2018**, *364*, 696−704.
(48) Roy, S. B.; Mondal, J.; Khuda-Bukhsh, A. R.; Rajak, K. K. A novel fluorene based "turn on" fluorescent sensor for the determination of zinc and cadmium: experimental and theoretical studies along with live cell imaging. *New J. Chem.* **2016**, *40*, 9593−9608.
(49) Jabeen, E.; Janjua, N. K.; Ahmed, S.; Murtaza, I.; Ali, T.; Masood, N.; Rizvi, A. S.; Murtaza, G. DFT predictions, synthesis, stoichiometric structures and anti-diabetic activity of Cu (II) and Fe

(III) complexes of quercetin, morin, and primuletin. *J. Mol. Struct.* **2017**, *1150*, 459−468.
(50) Maiti, P.; Saren, U.; Chakraborty, U.; Singha, T.; Paul, S.; Paul, P. K. Comparative and Selective Interaction of Amino Acid D-Cysteine with Colloidal Gold Nanoparticles in the Presence of a Fluorescent Probe in Aqueous Medium. *ACS Omega* **2022**, *7*, 29013−29026.
(51) Kasha, M.; Rawls, H. R.; El-Bayoumi, M. A. The exciton model in molecular spectroscopy. *Pure Appl. Chem.* **1965**, *11*, 371−392.
(52) Martinez, V. M.; Arbeloa, F. L.; Prieto, J. B.; Lopez, T. A.; Arbeloa, I. L. Characterization of Rhodamine 6G Aggregates Intercalated in Solid Thin Films of Laponite Clay. 1. Absorption Spectroscopy. *J. Phys. Chem. B* **2004**, *108*, 20030−20037.
(53) Gao, D.; Wang, Z.; Liu, B.; Ni, L.; Wu, M.; Zhang, Z. Resonance Energy Transfer-Amplifying Fluorescence Quenching at the Surface of Silica Nanoparticles toward Ultrasensitive Detection of TNT. *Anal. Chem.* **2008**, *80*, 8545−8553.
(54) Su, Q.; Jiang, C.; Gou, D.; Long, Y. Surface Plasmon-Assisted Fluorescence Enhancing and Quenching: From Theory to Application. *ACS Appl. Bio Mater.* **2021**, *4*, 4684−4705.
(55) Zhang, J.; Malicka, J.; Gryczynski, I.; Lakowicz, J. R. Surface-Enhanced Fluorescence of Fluorescein-Labeled Oligonucleotides Capped on Silver Nanoparticles. *J. Phys. Chem. B* **2005**, *109*, 7643−7648.
(56) Hergert, W.; Wriedt, T. *The Mie Theory: Basics and Applications*, Springer, 2012, DOI: 10.1007/978-3-642-28738-1.
(57) Cifuentes, A.; Bernal, J. L.; Diez-Masa, J. C. Determination of Critical Micelle Concentration Values Using Capillary Electrophoresis Instrumentation. *Anal. Chem.* **1997**, *69*, 4271−4274.
(58) Nie, W.; Zhu, Q.; Gao, Y.; Wang, Z.; Liu, Y.; Wang, X.; Chen, R.; Fan, F.; Li, C. Visualizing the Spatial Heterogeneity of Electron Transfer on a Metallic Nanoplate Prism. *Nano Lett.* **2021**, *21*, 8901−8909.
(59) AL-Aqmar, D. M.; Abdelkader, H. I.; Abou Kana, M. T. H. Spectroscopic properties and amplified spontaneous emission of fluorescein laser dye in ionic liquids as green media. *Opt. Mater.* **2015**, *47*, 573−581.
(60) Lakowicz, J. R.; Ray, K.; Chowdhury, M.; Szmacinski, H.; Fu, Y.; Zhang, J.; Nowaczyk, K. Plasmon-controlled fluorescence: a new paradigm in fluorescence spectroscopy. *Analyst* **2008**, *133*, 1308−1346.
(61) Bhaskar, S.; Srinivasan, V.; Ramamurthy, S. S. Nd_2O_3-Ag Nanostructures for Plasmonic Biosensing, Antimicrobial, and Anticancer Applications. *ACS Appl. Nano Mater.* **2023**, *6*, 1129−1145.
(62) Zhao, H.; Song, F.; Zhang, J.; Wang, F.; Liu, J.; Liu, Y. Fluorescence quenching of osthole by silver nanoparticles. *J. Opt. Soc. Am. B* **2013**, *30*, 2387−2392.
(63) Lakowicz, J. R. Radiative decay engineering 5: metal-enhanced fluorescence and plasmon emission. *Anal. Biochem.* **2005**, *337*, 171−194.
(64) Li, X.; Zhu, Y.; Cai, W.; Borysiak, M.; Han, B.; Chen, D.; Piner, R. D.; Colombo, L.; Ruoff, R. S. Transfer of Large-Area Graphene Films for High-Performance Transparent Conductive Electrodes. *Nano Lett.* **2009**, *9*, 4359−4363.
(65) Dutta Roy, S.; Ghosh, M.; Chowdhury, J. Near-Field Response on the Far-Field Wavelength-Scanned Surface Enhanced Raman Spectroscopic Study of Methylene Blue Adsorbed on Gold Nanocolloidal Particles. *J. Phys. Chem. C* **2018**, *122*, 10981−10991.
(66) Camden, J. P.; Dieringer, J. A.; Wang, Y.; Masiello, D. J.; Marks, L. D.; Schatz, G. C.; van Duyne, R. P. Probing the Structure of Single-Molecule Surface-Enhanced Raman Scattering Hot Spots. *J. Am. Chem. Soc.* **2008**, *130*, 12616−12617.
(67) Su, K. H.; Wei, Q. H.; Zhang, X.; Mock, J. J.; Smith, D. R.; Schultz, S. Interparticle Coupling Effects on Plasmon Resonances of Nanogold Particles. *Nano Lett.* **2003**, *3*, 1087−1090.
(68) Stuart, H. R.; Hall, D. G. Enhanced Dipole-Dipole Interaction between Elementary Radiators Near a Surface. *Phys. Rev. Lett.* **1998**, *80*, 5663−5666.
(69) Das, S.; Chattopadhyay, A. P.; De, S. Controlling J aggregation in fluorescein by bile salt hydrogels. *J. Photochem. Photobiol., C* **2008**, *197*, 402−414.
(70) Massoud, T. F.; Gambhir, S. S. Molecular imaging in living subjects: seeing fundamental biological processes in a new light. *Genes Dev.* **2003**, *17*, 545−580.
(71) Gao, Z.; Hao, Y.; Zheng, M.; Chen, Y. A fluorescent dye with large Stokes shift and high stability: synthesis and application to live cell imaging. *RSC Adv.* **2017**, *7*, 7604−7609.
(72) Capehart, S. L.; Coyle, M. P.; Glasgow, J. E.; Francis, M. B. Controlled Integration of Gold Nanoparticles and Organic Fluorophores Using Synthetically Modified MS2 Viral Capsids. *J. Am. Chem. Soc.* **2013**, *135*, 3011−3016.
(73) Atale, N.; Gupta, S.; Yadav, U. C. S.; Rani, V. Cell-death assessment by fluorescent and nonfluorescent cytosolic and nuclear staining techniques. *J. Microsc.* **2014**, *255*, 7−19.
(74) Gautier, A.; Hinner, M. J. *Site-Specific Protein Labeling: Methods and Protocols*; Springer, 2015.
(75) Austin, L. A.; Kang, B.; Yen, C. W.; El-Sayed, M. A. Plasmonic Imaging of Human Oral Cancer Cell Communities during Programmed Cell Death by Nuclear-Targeting Silver Nanoparticles. *J. Am. Chem. Soc.* **2011**, *133*, 17594−17597.
(76) Carlson, C.; Hussain, S. M.; Schrand, A. M.; Braydich-Stolle, L. K.; Hess, K. L.; Jones, R. L.; Schlager, J. J. Unique Cellular Interaction of Silver Nanoparticles: Size-Dependent Generation of Reactive Oxygen Species. *J. Phys. Chem. B* **2008**, *112*, 13608−13619.
(77) Behzadi, S.; Serpooshan, V.; Tao, W.; Hamaly, M. A.; Alkawareek, M. Y.; Dreaden, E. C.; Brown, D.; Alkilany, A. M.; Farokhzad, O. C.; Mahmoudi, M. Cellular uptake of nanoparticles: journey inside the cell. *Chem. Soc. Rev.* **2017**, *46*, 4218−4244.

https://doi.org/10.1021/acs.langmuir.3c00204
Langmuir 2023, 39, 6713−6729